



ESA Sea Level CCI

D2.6 Algorithm Theoretical Basis Document (ATBDv1)

Reference: CLS-SLCCI-16-0008
Nomenclature: SLCCI-ATBDv1-016
Issue: 3.3
Date: Aug. 23, 16





Chronology Issues:			
Issue:	Date:	Reason for change:	Author
1.0 (D2.3 ATBDv0)	15/01/11	Creation of ATBDv0 Issue 1.0	M.Ablain
1.0 (D2.6 ATBDv1)	22/06/12	Update of Algorithm Theoretical Basis Document after selecting algorithm selection meeting.	M.Ablain
2.0	19/12/12	Update of Algorithm Theoretical Basis Document in order to take into account feedbacks from ESA	M.Ablain
2.1	20/05/12	Corrections after ESA review	M.Ablain
3.0	27/01/16	Update of Algorithm Theoretical Basis Document consistent with ECV 2.0	L. Zawadzki
3.1	14/04/16	Update of Algorithm Theoretical Basis Document consistent with ECV 2.0 and GPD+ description	J. Fernandes
3.2	25/07/16	Update in response to ESA's review	J-F Legeais
3.3	23/08/16	Update in response to ESA's 2 nd review	L. Zawadzki

People involved in this issue:		
Written by (*):	M. Ablain; L. Zawadzki (CLS)	Date + Initials: (visa or ref)
Checked by (*):	S. Mbajon (CGI)	Date + Initial: (visa ou ref)
Approved by (*):	JF Legeais (CLS)	Date + Initial: (visa ou ref)
Application authorized by (*):	J. Benveniste (ESA)	Date + Initial: (visa ou ref)

**In the opposite box: Last and First name of the person + company if different from CLS*

Index Sheet:	
Context:	SLcci project ECV 2.0
Keywords:	Oceanography, sea level
Hyperlink:	

Distribution:		
Company	Means of distribution	Names
CLS	Notification	J. Benveniste, A. Ambrozio (ESA)



List of tables and figures

List of tables:

Tab. 1- New altimeter standards selected for the sea-level calculation in SL-CCI project.....	2
Tab. 2 - List of ATBDs corresponding to each algorithm	4

List of figures:

Figure 3.1 - Computation of the orbit altitude and the orbital altitude rate with respect to the reference ellipsoid	7
Figure 4.1 - Location of GNSS stations used in the GPD+ estimations. The background picture is the map of the standard error of the wet tropospheric correction, in metres, computed from two years of ECMWF model fields.....	11
Figure 4.2 - Set of Si-MWR sensors used in the GPD+ estimations (F08 and F15 were not used due to their instable behavior (Wentz, 2013)).	12
Figure 4.3 - Differences in WTC (cm) from SSM/I, SSM/IS and MWR on board satellite altimetry reference missions, before and after calibration.	13
Figure 4.4 - Spatial correlation scales (in km) for the WTC as determined from a set of ECMWF Operational Model grids at 0.125°x0.125° well distributed over the year 2013.....	15
Figure 4.5 - Location of Envisat cycle 62 (top) and TP cycle 443 (bottom) points selected for the GPD computation (points with flag_MWR_rej ≠ 0). Dark green: points with radiometer land flag set to 1; Light green: points with distance from coast less than a given threshold; Blue: points contaminated by ice; Pink: points rejected by outlier detection criteria or with the MWR WTC outside limits; Brown: land points near the coast (see text for details).	17
Figure 4.6 - Formal error (in cm) of the GPD wet tropospheric correction for Envisat cycle 62.	17
Figure 6.1- Illustration of the 5-dimensional TEC climatology. The foreground shows the monthly and 2-hourly global grids at times of high solar activity (GTEC is 70 TECU). In the background are the solutions for low solar activity (GTEC is 10 TECU).	23
Figure 6.2 - The red dots denote the TEC near Greenwich at 20:00 UTC according to JPL GIM. The blue line is the climatological fit. The residuals have an RMS of 2.6 TECU. The grey region represents the model's TEC range for GTEC values between 10 and 70.	23
Figure 6.3 - Examples of model results and measurements of TEC (left ordinate) and Ku-band ionosphere delay (right ordinate) along two long ocean-only passes across the Atlantic. Dots indicate dual-frequency altimeter measurements. The model results from GIM, NIC09 and IRI2007 are shown as lines. The numbers in the legends indicate the RMS difference between the measurements and models. Top: TOPEX and Jason-1, 6 Mar 2002 around 15:00 UTC. Bottom: Envisat, 20 Dec 2002 around 12:00 UTC.	24
Figure 6.4 - Global RMS difference between the results from various models and the dual-frequency altimeter measurements of TOPEX and Jason-1.....	25

Applicable documents

AD 1 Sea level CCI project Management Plan
CLS-DOS-NT-10-013



Reference documents

RD 1 PVSAR: Selection Meeting Report
CLS-DOC-NT-12-125



Acronyms List

ADT	Absolute Dynamic Topography
AMR	Advanced Microwave Radiometer (onboard Jason-2)
AMSR	Advanced Microwave Scanning Radiometer
AMSU	Advanced Microwave Sounding Unit
ATBD	Algorithm Theoretical Basis Document
COASTALT	Project on "Development of Radar Altimetry Data Processing in the Coastal Zone"
COG	Centre Of Gravity
CORSSH	Corrected Sea Surface Height AVISO products
DAC	Dry Atmospheric Correction
DAD	Dynamic Ancillary Data
DEM	Digital Elevation Model
DMSP	Defense Meteorological Satellite Program
DOI	Data Object Identifier
DT	Dry Troposphere
ECMWF	European Centre for Medium-range Weather Forecasts
EPM	EUREF Permanent Network
ERA	ECMWF ReAnalysis
ESA	European Space Agency
FES	Finite Element Solution Ocean tide model
GFO	Geosat Follow-On
GFZ	GeoForschungsZentrum in Potsdam, Germany
GIM	Global Ionosphere Maps
GNSS	Global Navigation Satellite System
GNSS	Global Navigation Satellite System
GPD	GNSS-derived Path Delay algorithm
GPRW	Gain Profile Range Window
GPS	Global Positioning System
GSFC	NASA's Goddard Space Flight Center
GTEC	GIM Total Electron Content
HK	Housekeeping
IGS	International GNSS Service
IRI	International Reference Ionosphere Models
ISP	Instrument Source Packets
JMR	Jason-1 Microwave Radiometer



JPL	Jet Propulsion Laboratory
LRM	Low Resolution Mode
LWE	Long Wavelength Errors
MADT	Map of Absolute Dynamic Topography
MDS	Measurement Data Set
MSLA	Mean Sea Level Anomalies
MSS	Mean Sea Surface
MWR	MicroWave Radiometer
NA	Not Applicable
NOAA	National Oceanic and Atmospheric Administration
NRT	Near Real Time
NTC	Non Time Critical
OA	Object Analysis
OB	On-Board
OSTST	Ocean Surface Topography Science Team
POD	Precise Orbit Determination
POE-E	Precise Orbit Estimation version 'E'
PTR	Point Target Response
RD	Reference Document
RMS	Root Mean Square
RTN	Real Time Navigation
SAD	Static Ancillary Data
SAR	Synthetic Aperture radar
SLA	Sea level Anomalies
SLCCI	Sea Level Climate Change Initiative
SLOOP	A Step forward alTtimetry Open Ocean Products
SLP	Sea Level Pressure
SI MWR	Scanning Imaging Microwave Radiometer
SRAL	SAR Radar Altimeter
SSB	Sea State Bias
SSH	Sea Surface Height
SSM/I	Special Sensor Microwave/Imager
Static IB	Static Inverse Barometer
STC	Short Time Critical
STM	Surface Topography Mission
TAI	International Atomic Time
TCWV	Total Column Water Vapour
TECU	10^{16} electrons/m ²
TG	Tidal Gauge
TMI	TRMM Microwave Imager



TP	TOPEX Satellite
TRMM	Tropical Rainfall Measuring Mission
UTC	Coordinated Universal Time
WTC	Wet Tropospheric Correction
ZHD	Zenith Hydrostatic Delay
ZTD	Total Tropospheric Correction
ZWD	Zenith Path Delay
ATBD	Algorithm Theoretical Basis Document
COG	Centre Of Gravity
ECMWF	European Centre for Medium-range Weather Forecasts
ERA	ECMWF ReAnalysis
GNSS	Global Navigation Satellite System
GPD	GNSS-derived Path Delay algorithm
GPRW	Gain Profile Range Window
GPS	Global Positioning System
HK	Housekeeping
ISP	Instrument Source Packets
LRM	Low Resolution Mode
MDS	Measurement Data Set
MSLA	Mean Sea level Anomalies
MWR	MicroWave Radiometer
NA	Not Applicable
NRT	Near Real Time
NTC	Non Time Critical
OB	On-Board
POD	Precise Orbit Determination
PTR	Point Target Response
RD	Reference Document
RTN	Real Time Navigation
SAR	Synthetic Aperture radar
SRAL	SAR Radar Altimeter
SLA	Sea level Anomalies
SSB	Sea State Bias
STC	Short Time Critical
STM	Surface Topography Mission
TAI	International Atomic Time
ZWD	Zenith Path Delay



List of Contents

1. Overview	1
1.1. References	3
2. List of ATBDs	3
3. ATBD- 1: To compute orbit altitude	5
3.1. Selected altimeter standards.....	5
3.2. Function	5
3.3. Algorithm Definition	5
3.3.1. Input data	5
3.3.2. Output data	6
3.3.3. Mathematical statement	6
3.4. Accuracy.....	7
3.5. References	7
4. ATBD-2: To compute wet troposphere corrections from the GNSS-derived Path Delay (GPD+) algorithm	9
4.1. Selected altimeter standards.....	9
4.2. Function	10
4.3. Algorithm Definition	10
4.3.1. Input data	10
4.3.2. Output data	13
4.3.3. Mathematical statement	14
4.4. Accuracy.....	16
4.5. References	18
5. ATBD-3: To compute the sea state biases	19
5.1. Selected altimeter standards.....	19
5.2. Function	19
5.3. Algorithm Definition	19
5.3.1. Input data	19
5.3.2. Output data	19
5.3.3. Mathematical statement	19
5.4. Accuracy.....	19
5.5. References	20
6. ATBD-4: To compute ionosphere correction derived from Nic09 model	21
6.1. Selected altimeter standards.....	21
6.2. Function	21
6.3. Algorithm Definition	21
6.3.1. Input data	21



6.3.2. Output data	21
6.3.3. Mathematical statement	21
6.4. Accuracy.....	23
6.5. References	25
7. ATBD-5: To compute the high frequency fluctuations	26
7.1. Selected altimeter standards.....	26
7.2. Function	26
7.3. Algorithm definition.....	26
7.3.1. Input data	26
7.3.2. Output data	26
7.3.3. Mathematical statement	26
7.4. Accuracy.....	28
7.5. References	28
8. ATBD-6: Dry troposphere corrections derived from ERA-interim pressure fields	29
8.1. Selected altimeter standards.....	29
8.2. Function	29
8.3. Algorithm definition.....	29
8.3.1. Input data	29
8.3.2. Output data	30
8.3.3. Mathematical statement	30
8.4. Accuracy.....	33
8.5. References	33
9. ATBD-7: To compute ocean tide height (including long period equilibrium ocean tide) and load tide height.....	34
9.1. Selected altimeter standards.....	34
9.2. Function	34
9.3. Algorithm Definition	34
9.3.1. Input data	34
9.3.2. Output data	35
9.3.3. Mathematical statement	35
9.4. Accuracy.....	36
9.5. References	36
10. ATBD-8: To compute grid ECV products	37
10.1. Selected altimeter standards	37
10.2. Function	37
10.3. Algorithm Definition.....	37
10.3.1. Input data	37



10.3.2. Output data.....	37
10.3.3. Mathematical statement.....	37
10.4. References	39
11. ATBD-9: To compute the mean sea surface height	40
11.1. Selected altimeter standards	40
11.2. Function	40
11.3. Algorithm Definition	40
11.3.1. Input data	40
11.3.2. Output data.....	40
11.3.3. Mathematical statement.....	41
11.4. References	41



1. Overview

The objective of this document is to define the Algorithm Theoretical Basis Document (ATBD) for all the algorithms used to compute the altimeter standards along the 1Hz altimeter measurements. Altimeter standards are the components used in the SSH calculation defined by this formula:

$$SLA = Orbit - Range - \sum_{i=0}^N C_i - MSS \quad \text{Eq 1.1}$$

where *Orbit* corresponds to the distance between the satellite and the ellipsoid, *Range* is the distance measured by the altimeter between the satellite and the sea surface, *MSS* is the Mean Sea Surface of the ocean over a long period and $\sum_{i=0}^N C_i$ is the sum of all the corrections needed to take into account the atmospheric effects (wet and dry troposphere, ionosphere, inverse barometer), the geophysical phenomena (ocean tides, high frequency atmospheric effects on ocean) and the sea-surface state (electromagnetic sea-surface bias).

During the “Selection Meeting” held in Toulouse on 2-4 May 2012, the best altimeter standards developed in SLCCI project (WP2) at the time were selected in order to calculate the sea-level for climate studies. The selected corrections have been described in the corresponding version of RD1 document (PVSAR: Selection Meeting Report). Then, during the “Selection Meeting” held in Toulouse on 26-27 November 2015, new altimeter standards have been selected in order to upgrade the SL_cci ECV v1.1 to ECV v2.0. The selected altimeter standards have been displayed in Tab. 1.

In this document, the description of algorithms needed to calculate these corrections along the 1Hz altimeter measurements (depending on location: time, latitude, longitude) is reported.



Mission	ERS-1	ERS-2	EnviSat	TOPEX/ Poseidon	Jason-1	Jason-2	GFO	SARAL/ AltiKa	CryoSat-2
Orbit	GFZ 2015			GSFC STD15 (cycle 1-374), STD 12 from cycle 374	POE-E		GSFC	POE-E	
Sea State Bias	3-parameter (Gaspar, Ogor, 1994)	Non parametric Mertz et al., 2005	Non parametric SSB [N. Tran 2015]	Non parametric SSB [N. Tran and al. 2010]	Non parametric SSB [N. Tran and al. 2012]	Non parametric SSB [N. Tran and al. 2012]	Non parametric SSB [Tran and Labroue, 2009]	SSB PEACHI 2014 2D	Non parametric SSB from J1
Ionosphere	NIC09	NIC09 (cycle 1-49), GIM from cycle 50	Iono SLOOP filter / GIM (GDR2.1)	Iono SLOOP filter			GIM		
Wet troposphere	GPD+						GFO radiometer + ECMWF	GPD+	
Dry troposphere	Era Interim based								
Combined atmospheric correction	Era Interim based								
Ocean tide	FES 2014 (including ocean tides, long period equilibrium tide, S1 tides...)								
Load tide	GOT4V8 AC [Ray, 2013]								
Solid Earth tide	Elastic response to tidal potential [Cartwright and Tayler, 1971], [Cartwright and Edden, 1973]								
Pole tide	[Desai et al., 2015]								
MSS	DTU15								
Major instrumental correction			USO correction correcting for anomaly periods and aging drift from auxiliary files						

Tab. 1- New altimeter standards selected for the sea-level calculation in SL-CCI project.



1.1. References

Cartwright and Edden, 1973. Corrected Tables of Tidal Harmonics. Geophysical Journal international, 33, 3, 253-264.

Cartwright and Tayler, 1971. New computations of the Tide-generating Potential. Geophysical Journal international, 23, 1 45-73.

Desai S., J. Wahr and B. Beckley, 2015. Revisiting the pole tide for and from satellite altimetry. J. Geod., 89(12), 1233-1243. doi: 10.1007/s00190-015-0848-7.

Gaspar, P. et Ogor, F., Estimation and analysis of the sea state bias of the ers-1 altimeter. Rapport technique, Report of task B1-B2 of IFREMER Contract n° 94/2.426 016/C. 84, 1994.

Mertz F., F. Mercier, S. Labroue, N. Tran, J. Dorandeu, 2005: ERS-2 OPR data quality assessment; Long-term monitoring - particular investigation. CLS.DOS.NT-06.001. http://www.aviso.altimetry.fr/fileadmin/documents/calval/validation_report/E2/annual_report_e2_2005.pdf. (last access: 11 May 2016)

Ray, R. D., 2013, "Precise Comparisons of bottom-pressure and altimetric ocean tides", J. of Geophys. Res. (Oceans), 118, 4570-4584.

Tran N. and S. Labroue, 2009. Personal communication.

Tran N., S. Labroue, S. Philipps, E. Bronner and N. Picot, 2010. Overview and update of the sea state bias corrections for the Jason-2, Jason-1 and TOPEX missions. Marine Geodesy, 33(S1): 348-362, 2010. DOI: 10.1080/01490419.2010.487788.

Tran, N., S. Philipps, J-C. Poisson, S. Urien, E. Bronner, et N. Picot. 2012 "Oral: Impact of GDR-D standards on SSB corrections.", Aviso, OSTST. http://www.aviso.altimetry.fr/fileadmin/documents/OSTST/2012/oral/02_friday_28/01_instr_processing_1/01_IP1_Trان.pdf

Tran N. 2015. Envisat Phase-F: Sea State Bias", Technical Report CLS-DOS-NT-15-031, ESA contract "ENVISAT RA-2 AND MWR ESL AND PROTOTYPES MAINTENANCE SUPPORT (LEVEL 1B AND LEVEL 2).

2. List of ATBDs

In the following table the list of ATBDs corresponding to each algorithm is presented. The number and a short description of the algorithm are listed for each ATBD. The correspondent altimeter standards used in the SSH calculation are also described. Each ATBD is presented in detail in the following chapters.

ATBD Number	Algorithm Description	Altimeter standards	Pages
ATBD-1	To compute orbit altitude	GFZ orbit solutions	Page 5
		CNES POE-E orbit solutions	
		GSFC orbit solutions	
ATBD-2	To compute Wet troposphere correction from GNSS-derived Path Delay (GPD+)	GNSS-derived Path Delay, Scanning Imager calibrated (GPD+) algorithm	Page 9
ATBD-3	To compute the sea state biases	Sea State Bias Non-parametric solution	Page 19
ATBD-4	To compute ionosphere correction	Ionosphere correction derived from the NIC09 model	Page 21



ATBD-5	To compute the high frequency fluctuations	Dynamical atmospheric correction derived from ERA-interim model	Page 26
ATBD-6	Dry troposphere derived from ERA-interim pressure fields	Dry troposphere derived from ERA-interim pressure fields	Page 29
ATBD-7	To compute elastic ocean tide height and the load tide height	FES2014 ocean tide model	Page 34
ATBD-8	To compute the mean sea surface height	DTU15 Mean Sea Surface	Page 40

Tab. 2 - List of ATBDs corresponding to each algorithm



3. ATBD- 1: To compute orbit altitude

3.1. Selected altimeter standards

For ERS-1, ERS-2, ENVISAT: The GFZ orbit solutions have been selected.

For Jason-1, Jason-2, SARAL/AltiKa, CryoSat-2: CNES POE-E orbit solutions have been selected

For TOPEX/Poseidon: GSFC STD1504 orbit solution has been selected for cycles 1-374, followed by GSFC STD1204 from cycle 375 onwards.

Name	Description	Mission applicability
GFZ orbit solutions	The GFZ orbit solution has been provided by GFZ in the framework of the SLcci project. For more information see Sergei Rudenko's talk (OSTST 2015, Reston)	ERS-1, ERS-2, EnviSat
CNES POE-E orbit solutions	The CNES POE-E orbit has been provided by CNES in the framework of the SALP project. For more information see Eva Jalabert's talk(OSTST 2015, Reston).	Jason-1, Jason-2, SARAL/AltiKa, CryoSat-2
GSFC STD1504 and STD1204 orbit solutions	The GSFC orbit solution is available on cddis.gsfc.nasa.gov website. For more information, see Frank Lemoine's talk (OSTST 2015, Reston).	TOPEX/Poseidon

3.2. Function

To compute the orbit altitude (i.e. the altitude of the platform center of gravity above the reference ellipsoid), the orbital altitude rate (i.e. the height rate [m/s] of the satellite at a specific time used to compute the Doppler correction on the altimeter range¹) with respect to the reference ellipsoid and the location of the measurements from orbit files.

3.3. Algorithm Definition

3.3.1. Input data

- Datation:
 - 1-Hz altimeter time tag
 - Information to derive the elementary time tags (offset to derive the time-tag of the first elementary measurement, and time interval between two elementary measurements)
- Orbit (DAD):
 - Orbit data covering the time span of the input product, i.e. at regular time steps:

¹ taken from: <https://sentinel.esa.int/web/sentinel/sentinel-3-altimetry-wiki/-/wiki/Sentinel+Three+Altimetry/Orbital+Altitude+Rate;jsessionid=437F472CC6B9704674092D3809BDE4B3.eodisp-prod4040>



- Position of the satellite in a terrestrial reference frame: $\vec{P} = (P_X, P_Y, P_Z)$
- Velocity of the satellite in a terrestrial reference frame: $\vec{V} = (V_X, V_Y, V_Z)$
- Processing parameters (SAD):
 - Processing parameters for the orbit interpolation
 - Processing parameters for the determination of the orbit altitude and of the latitude (iterative process): desired accuracy for the orbit altitude, desired accuracy for the latitude
- Universal constants (SAD):
 - Flattening coefficient of the reference ellipsoid
 - Semi major axis of the reference ellipsoid

3.3.2. Output data

- Orbit altitudes
- Orbital altitude rates
- Location, i.e. latitude and longitudes

3.3.3. Mathematical statement

- The orbit altitude h , the latitude φ and the longitude λ corresponding to an input 20-Hz or 1-Hz altimeter time-tag t , are computed as follows:
 - N (typically $N=8$) position vectors are selected from the input orbit file ($N/2$ before and $N/2$ after the altimeter time tag), and are interpolated at the altimeter time tag using Everett's formula (Abramowitz, 1965).
 - The interpolated position $\vec{P}_S = (P_{SX}, P_{SY}, P_{SZ})$ of the satellite is then projected onto the reference ellipsoid to provide h , φ and λ (see Nouel, 1980 or Klinkrad, 1985 or Guinn, 1990).
- The orbital altitude rate with respect to the reference ellipsoid (h') corresponding to an input 20-Hz or 1-Hz altimeter time-tag t is computed as follows, using the corresponding latitude φ and longitude λ (computed as defined above):
 - The position $\vec{P}_N = (P_{NX}, P_{NY}, P_{NZ})$ of the geodetic subsatellite point (denoted as the nadir point) is derived from φ and λ , using a simple change of co-ordinate system (see Nouel, 1980).
 - The normalized line of sight vector, in the direction NS defined by the satellite (S) and the corresponding nadir point (N) is then computed by:

$$\vec{L} = \frac{\vec{P}_S - \vec{P}_N}{\|\vec{P}_S - \vec{P}_N\|} \quad \text{Eq 3.1}$$

- M (typically $M=8$) velocity vectors are selected from the input orbit file ($M/2$ before and $M/2$ after the altimeter time tag), and are interpolated at the altimeter time tag using Everett's formula (Abramowitz, 1965).
- The orbital altitude rate h' is finally obtained by forming a scalar product of the interpolated satellite velocity vector $\vec{V}_S = (V_{SX}, V_{SY}, V_{SZ})$ with the normalized line of sight vector \vec{L} (Dumont et al., 1997), i.e. by:



$$h' = \frac{V_{SX} \cdot (P_{SX} - P_{NX}) + V_{SY} \cdot (P_{SY} - P_{NY}) + V_{SZ} \cdot (P_{SZ} - P_{NZ})}{\sqrt{(P_{SX} - P_{NX})^2 + (P_{SY} - P_{NY})^2 + (P_{SZ} - P_{NZ})^2}} \text{ m/s} \quad \text{3.3.3.1.1.1.1.1. Eq. 3.2}$$

- The points and vectors used in the above descriptions are illustrated in **Figure 3.1**

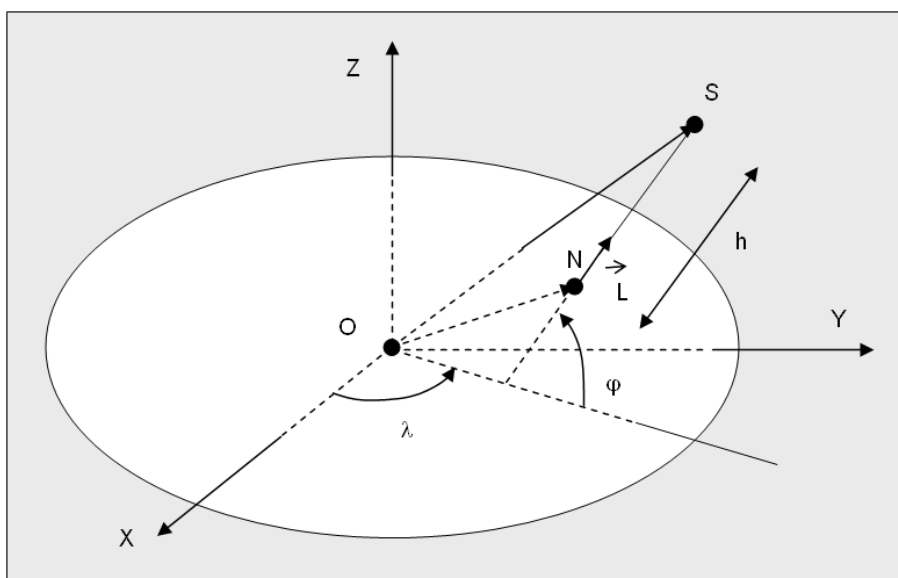


Figure 3.1 - Computation of the orbit altitude and the orbital altitude rate with respect to the reference ellipsoid

3.4. Accuracy

The error due to Everett interpolation method is smaller than 1 mm if the number N of orbit points taken into account is large enough (typically N=8, i.e. 4 points before and 4 points after the altimeter time) (Dumont et al., 1997).

3.5. References

- Abramowitz M. And Stegun I.A., Handbook of Mathematical Functions, Dover Publication Inc. N.Y., 1965
- Dumont J.-P., J. Stum and O. Z. Zanife, 1997. Algorithms Definition and Accuracy, RA2/MWR LOP, CLS.OC/NT/96.038, Issue 2rev1, 14 November 1997, Nomenclature : PO-NT-RAA-0004-CLS, http://envisat.esa.int/support-docs/pdf/ra2mwr_ada.pdf
- Noel, F., Les Repères de l'Espace et du Temps, Le Mouvement du Véhicule Spatial en orbite, Cours de Technologie Spatiale, CNES, 1980.
- Klinkrad, H., ERS-1, Algorithms for orbit prediction and for the determination of related static and dynamic altitude and groundtrace quantities, ESA, ER-RP-ESA-SY-0001, 1985.
- Guinn, J.R., Definition of Reference Earth Ellipsoid for TOPEX/POSEIDON, JPL Interoffice Memorandum, 314.5-1409, 15 February 1990.





4. ATBD-2: To compute wet troposphere corrections from the GNSS-derived Path Delay (GPD+) algorithm

4.1. Selected altimeter standards

The wet tropospheric path delay is almost proportional to the integrated water vapour content of the atmosphere and strongly affects the range measured by the altimeter (up to 50 cm). Meteorological models do not properly describe the high water vapour variability in space and time, therefore a dedicated microwave radiometer is added to the mission. The GPD+ algorithm has been selected for the estimation of the wet tropospheric correction for climate applications, for all missions with an onboard MWR (except for GFO, for which this correction has not been computed) and for CryoSat-2 (not equipped with an onboard MWR).

Name	Description	Mission applicability
GNSS-derived Path Delay Plus (GPD+) algorithm	<p>Main features of the GPD+ algorithm:</p> <ul style="list-style-type: none"> • The GPD+ are wet path delays based on: i) WTC from the on-board microwave radiometer (MWR) measurements whenever they exist and are valid; ii) new WTC values estimated by data combination, through space-time objective analysis (OA) of all available data sources, whenever the previous are considered invalid. • In the estimation of the new WTC values, the following data sets are used: valid measurements from the on-board MWR, from water vapour products derived from a set of near 20 scanning imaging radiometers (SI-MWR) on board various remote sensing satellites and wet path delays derived from GNSS (Global Navigation satellite Systems) coastal and island stations. • In the estimation process, WTCs derived from an atmospheric model, such as the European Centre for Medium-range Weather Forecasts (ECMWF) ReAnalysis (ERA) Interim or the operational (Op) model, are used as first guess and adopted in the absence of measurements. • At each altimeter point with an invalid MWR value, the wet tropospheric correction is estimated, along with the associated mapping error, using a linear space-time objective analysis technique that takes into account the spatial and temporal variability of the wet path delay field and the accuracy of each data set used. • All radiometer data sets have been inter-calibrated, using the set of Sensor Microwave Imager (SSM/I) and SSM/I Sounder (SSM/IS) on board the Defense Meteorological Satellite Program (DMSP) satellite series (FXX) as reference. 	ERS-1, ERS-2, EnviSat, TOPEX/Poseidon, Jason-1, Jason-2, SARAL/AltiKa, CryoSat-2



4.2. Function

The initial aim of this algorithm was to provide the wet tropospheric correction in the coastal zone, where the MWR measurements become invalid due to land contamination in the radiometer footprint (~25 km). In the present implementation the WTC is provided globally for all altimeter ocean measurements.

Whenever an MWR measurement is considered valid, the correction equals the MWR-based wet path delay. For every ocean point along the altimeter ground track for which the MWR-based WTC has been considered invalid according to a set of criteria, a new estimate is obtained along with its associated error. These include not only coastal points, but also open ocean, including high latitudes. Therefore, apart from land contamination, rain and ice contamination are also spotted and corrected.

The algorithm ensures the continuity and consistency of the correction in the open-ocean / coastal transition zone and also at high latitudes.

Moreover, the calibration with respect to the SSM/I and SSM/IS set of sensors ensures the temporal consistency between missions, due to the well-known stability and independent calibration of these sensors.

In phase II of the project the corrections were computed for the following 8 missions: ERS-1 (E1), ERS-2 (E2), EnviSat (EN), TOPEX/Poseidon (TP), Jason-1 (J1), Jason-2 (J2), SARAL/AltiKa (SA) and CryoSat-2 (C2).

4.3. Algorithm Definition

4.3.1. Input data

- 1) Wet path delays from valid MWR measurements at the nearby locations around the point of estimation. Due to the time difference between adjacent satellite tracks, in practice only points from a single track are used, the track to which the point of estimation belongs. The baseline MWR data used for the various missions are:
 - ERS-1 and ERS-2 - MWR data based on the ESA Ocean Product (OPR) modified by the algorithms discussed in Scharroo et al. (2004), available in the Radar Altimeter Database System (RADS);
 - Envisat - MWR Reprocessing V3.0, a recent correction provided by CLS (CLS personal communication);
 - TOPEX/Poseidon - Topex Microwave Radiometer (TMR) replacement product (http://podaac.jpl.nasa.gov/dataset/TOPEX_L2_OST_TMR_Replacement) available in RADS;
 - Jason-1 - MWR values present in the AVISO CORSSH products (JMR Replacement product changed by the Composite algorithm in the band 0-50 km around the coast). For use in the GPD+ estimations, on top of the usual analysis for identification of invalid MWR values, all points in the band 0-50 km from coast were flagged as invalid and estimated. The reason for adopting this Jason-1 MWR product is to remove the “anomaly” detected in the JMR Enhanced product used in the previous GPD WTC versions;
 - Jason-2 - AMR GDR-D product, already enhanced near the coast, Brown (2010);
 - SARAL/AltiKa - the most recent on-board MWR product, available in the PEACHI products.
- 2) Zenith wet delays (ZWD) derived at a network of coastal GNSS stations. GNSS data from about 800 stations were used (Figure 4.1). These include zenith total delays (ZTD) computed



at UPorto and ZTDs available online at a set of stations from IGS (International GNSS Service), EPN (EUREF Permanent Network), SuomiNet and from the German Bight provided by the Technische Universität Darmstadt in the scope of this project. Only stations up to 100 km from the coast and with an orthometric height < 1000 m were considered. The first condition aims at selecting only coastal stations; the second is due to the fact that the expression for the height dependence of the WTC by Kouba (2008), used to reduce the ZWD from Station height to sea level, is valid only up to 1000m.

The quantity estimated at each GNSS station is the total tropospheric correction (ZTD) at station level given by the sum of the zenith hydrostatic delay (ZHD) and zenith wet delay (ZWD) though appropriate mapping functions related to the angle of elevation. The quantity used in coastal altimetry is the ZWD at sea level. The latter is obtained from the ZTD at station level by computing the dry correction or zenith hydrostatic delay (ZHD) from the ERA Interim SLP (Sea Level Pressure) field using the Saastamoinen model (Davis et al., 1985) and reducing ZHD and ZWD fields to sea level using the procedure by Kouba (2008), with the modifications introduced by Fernandes et al. (2015).

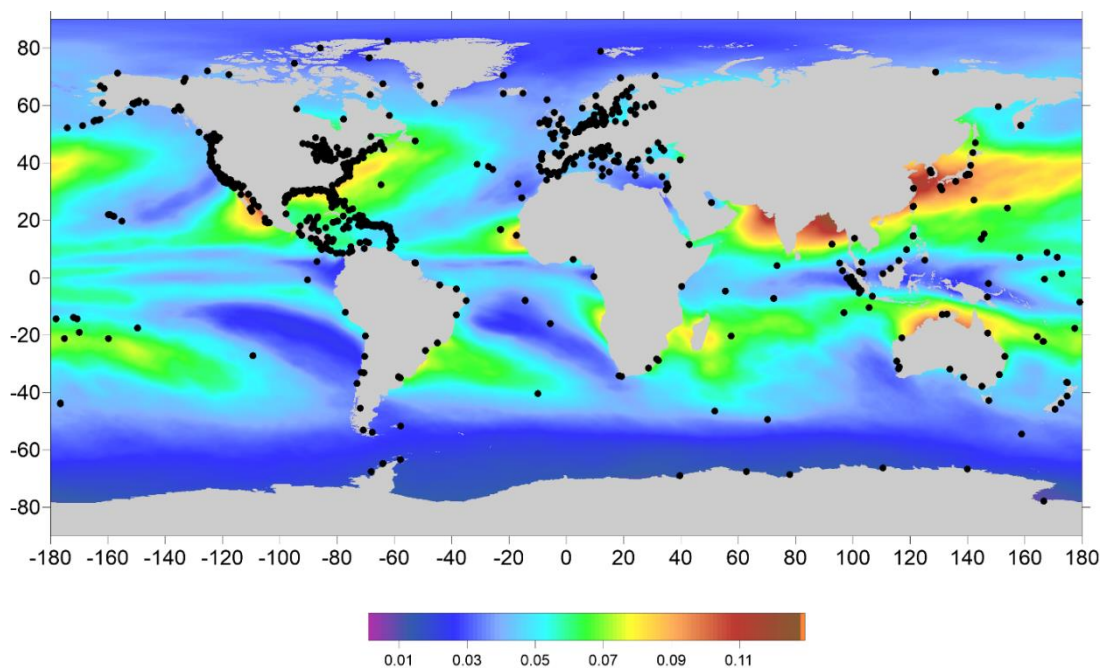


Figure 4.1 - Location of GNSS stations used in the GPD+ estimations. The background picture is the map of the standard error of the wet tropospheric correction, in metres, computed from two years of ECMWF model fields

- 3) Water vapour products from a set of 17 scanning imaging radiometers on board various remote sensing satellites available from two main sources: NOAA CLASS System (AMSU on NOAA-15, 16, 17, 18, 19, MetOp-A and MetOp-B) and Remote Sensing Systems (AMSR-E on Aqua, AMSR-2 on GCOM-W, WindSat on Coriolis, TMI on TRMM, SSM/I on DMSP satellites F10, F11, F13, F14, SSM/IS on F16, F17), see figure 4.2.

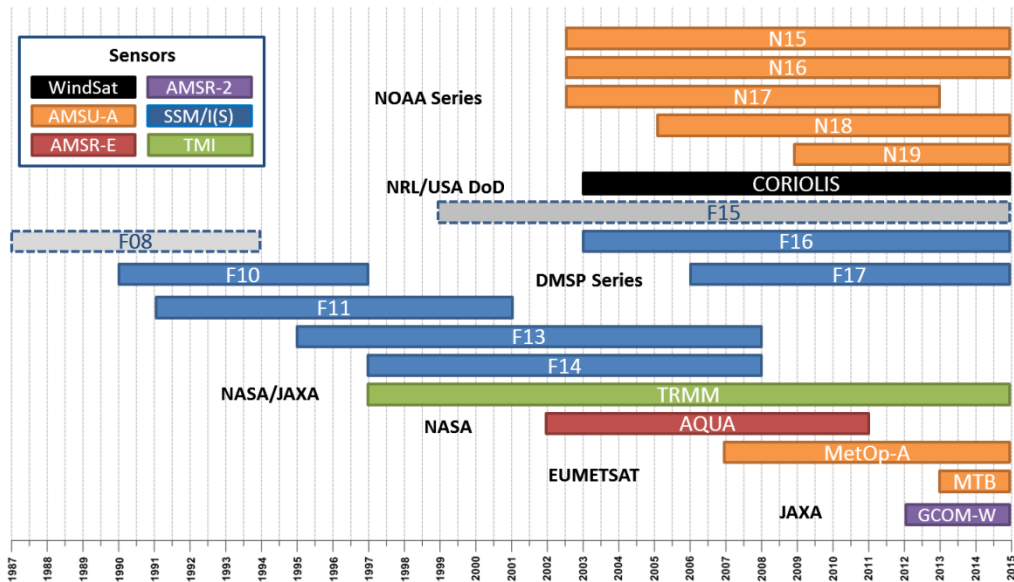


Figure 4.2 - Set of Si-MWR sensors used in the GPD+ estimations (F08 and F15 were not used due to their instable behavior (Wentz, 2013)).

- 4) Tropospheric delays from the European Centre for Medium-range Weather Forecasts (ECMWF) operational model (used for the most recent missions: Jason-2, CryoSat-2 and SARAL) and from the ERA Interim, used for the remaining missions.

ECMWF provides global $0.125^\circ \times 0.125^\circ$ (Operational model) or $0.75^\circ \times 0.75^\circ$ (ERA Interim) grids of several atmospheric parameters every 6 hours (Miller et al., 2010, Dee et al., 2011). In the scope of this study, the atmospheric fields of three single-level parameters of the two aforementioned models were used for the period [1991 - 2015] and for the whole globe:

- Sea level pressure (SLP)
- Surface temperature (2-meter temperature, 2T)
- Integrated water vapour (Total Column Water Vapour, TCWV)

These parameters are used both in the ZWD processing described above and to compute a model-derived WTC for each altimeter along-track position by space-time interpolation from the two closest grids, 6-hours apart. These model-derived WTC are used as first guess in the OA estimation and as adopted GPD+ values in the absence of observations.

Sensor calibration

To ensure consistency and the long term stability of the WTC, the large set of radiometers used in the GPD+ estimations have been inter-calibrated, using the set of SSM/I and SSM/IS on board the DMSP satellite series (F10, F11, F13, F14, F16 and F17) as reference, due to their well-known stability and independent calibration (Wentz, 2013). The calibration was performed in three steps:

- Step1 - TP, J1, J2 were calibrated against the FXX series
- Step2 - All 35-day missions were calibrated against TP, J1, J2
- Step3 - remaining SI-MWR were calibrated against TP, J1, J2

The adjustment model uses three parameters: Offset (a), scale factor (b) and trend (c):

$$Y = a + bX + c(T - T_0), \quad T_0 = 1992 \quad \text{Eq 4.1}$$

In step 1 match points between SSM/I and SSM/IS sensors and MWR on board reference altimetric mission (TP, J1, J2) were calculated. Only points with time difference $\Delta T < 45$ min and distance



$\Delta D < 50$ km were considered (Fernandes et al., 2013). The WTC data from each reference altimetric mission were then adjusted to the WTC data from SSM/I and SMM/IS set of sensors (Figure 4.3).

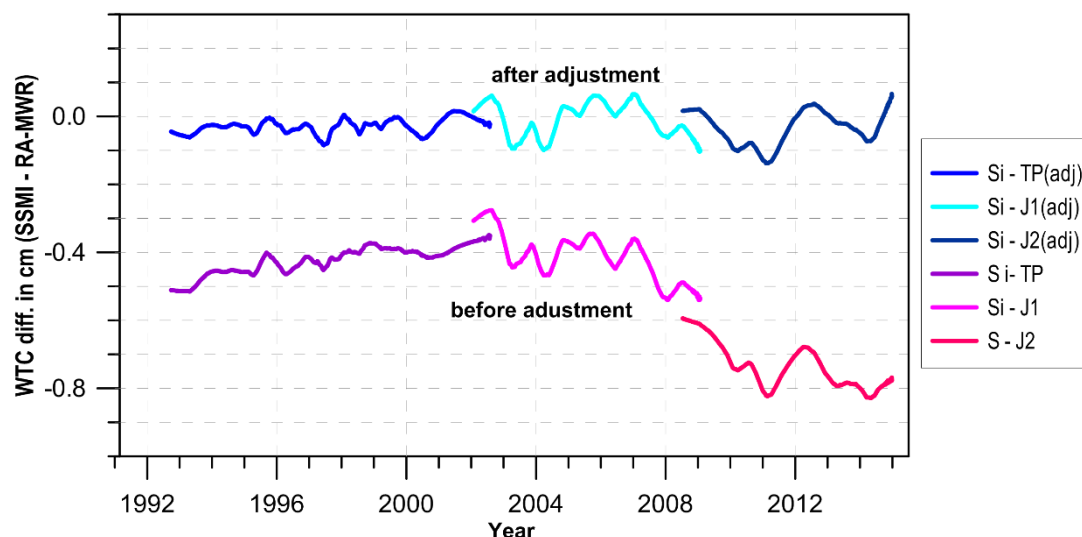


Figure 4.3 - Differences in WTC (cm) from SSM/I, SSM/IS and MWR on board satellite altimetry reference missions, before and after calibration.

In step 2 the WTC from each 35-day mission (E1, E2, EN, SA) were calibrated against the WTC from the reference missions (TP, J1, J2) by minimizing the crossover differences between each sun-synchronous 35-day mission and the altimetry reference missions. Only crossover points with a $\Delta T < 180$ min were considered. This value was found to be the best compromise between the number of crossovers and the minimum time interval.

In step 3 the WTC from all remaining SI-MWR (except the FXX series) sensors were adjusted to the WTC from the altimetric reference missions.

For the reference altimetric missions the offsets are in the range -0.8 to 0.6 cm, the scale factors in the range 0.96 to 0.99 and the trends in the range -0.22 to 0.15 mm/yr. For the 35-day altimetric missions the offsets are in the range -1.3 to 0.8 cm, the scale factors in the range 0.96 to 0.99 and the trends in the range 0.07 to 0.17 mm/yr. For the remaining SI-MWR the offsets are in the range -1.1 to 0.0 cm, the scale factors in the range 0.99 to 1.02 and the trends in the range -0.26 to 0.25 mm/yr. Although these parameters are generally small, they have an effect in the global sea level variation mainly at decadal time scales and in the regional mean sea level.

4.3.2. Output data

For each ocean and coastal measurement point along the satellite track, the output fields listed below are provided. In addition to ocean points, to help on interpolation to higher data rates, the first land point of each track is also selected, provided it is within 50 km from the coastline (brown points in Figure 4.5).

- wet_GPD** - wet tropospheric correction (metres)
- GPD_error** - formal error of the wet_GPD estimate (metres)
- GPD_flag** - validity flag of the wet_GPD estimate:
 - 0 - non-corrupted ocean points. For these wet_GPD = rad_wet_tropo_cor.
 - 1 - wet_GPD is a valid estimate.



2 - there were no observations to perform the GPD estimation. For these points wet_GPD is set to the model-derived WTC.

3 - Unreliable GPD estimate, according to algorithm internal criteria.

In practice, the wet_GPD wet tropospheric correction is valid when GPD_flag = 0, 1 or 2. For points with GPD_flag = 0 the correction is the original radiometer correction, possibly scaled due to sensor calibration (see text about sensor calibration above); for points with GPD_flag = 1 a valid estimate of the wet tropospheric correction has been obtained from the available observations; when GPD_flag = 2 the correction is the adopted model used as first guess in the estimation process.

4.3.3. Mathematical statement

The GNSS-derived Path Delay (GPD) methodology, developed at UPorto, started as a coastal algorithm in the scope of the ESA project COASTALT (Development of radar altimetry data processing in the oceanic coastal zone), aiming at removing the land effects in the microwave radiometers on board the altimeter missions (Fernandes et al., 2010). Then the methodology evolved to cover the open ocean, including high latitudes, correcting for invalid observations due to land, ice and rain contamination and instrument malfunction (Fernandes et al., 2015). After adequate algorithm tuning, it is applicable to any other altimetric mission with or without an on-board MWR.

The most recent version of this algorithm, designated GPD Plus (GPD+), developed in phase II of the SL_cci project, includes the previously designated GPD and DComb (Data Combination) algorithms, the latter developed for CryoSat-2 in the scope of the CP40 (CryoSat Plus for Oceans) project.

The core of the GPD algorithm is based on a linear space-time objective analysis (OA) technique (Bretherton et al., 1976). The statistical technique interpolates the wet path delay values at each altimeter ground-track point with invalid MWR measurements from the nearby (in space and time) observations. It updates a first guess value known a priori at each location and epoch and provides a quantification of the mapping error associated with each estimate.

Thus, the GPD+ are wet path delays based on: i) WTC from the on-board MWR measurements whenever they exist and are valid; ii) new WTC values estimated by data combination of all available observation in the vicinity of the estimation point, whenever the previous are considered invalid.

The spatial and temporal variability of the ZWD field is taken into account by the correlation function which, in the absence of the knowledge of an empirical covariance model of the background field, can take the form of a product of two stationary Gaussian decays (Leeuwenburgh, 2000; Schüler, 2001).

The space correlation scales were determined from a set of ECMWF operational model grids at $0.125^\circ \times 0.125^\circ$, well distributed over the year 2013. The computations were performed for a grid of points centered on $2^\circ \times 2^\circ$ "boxes". For each of these central points, analyses were made on boxes of $2^\circ \times \Delta\lambda^\circ$, where $\Delta\lambda = \min(2^\circ / \cos \varphi, 2^\circ)$, where φ and λ stand for latitude and longitude, respectively. This warrants that all analyses are made on boxes of approximately the same size. For each box, the correlation between all pairs of points separated by a distance R, for classes of R spaced by 10 km, were determined. The set (R, corr(R)) forms the correlation table for each box. The corresponding correlation scale D is obtained by either fitting a Gaussian function to the correlation table or by computing the value of R corresponding to a correlation equal to $1/e$. Both approaches give similar results and the resulting spatial correlation scales are within 40 to 93 km (Figure 4.4).

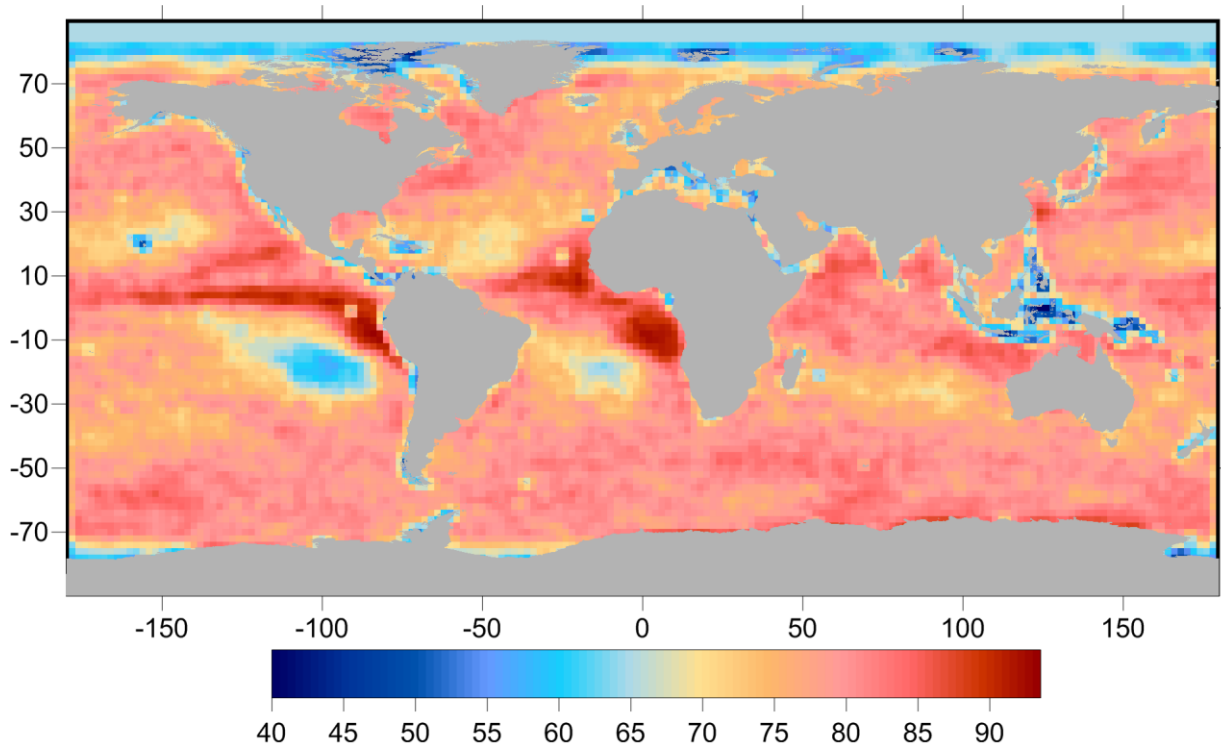


Figure 4.4 - Spatial correlation scales (in km) for the WTC as determined from a set of ECMWF Operational Model grids at $0.125^\circ \times 0.125^\circ$ well distributed over the year 2013.

For the temporal correlation scales, in the absence of time to perform a similar analysis within the time frame of this project, the value of 100 minutes quoted by Bosser et al. (2007) was adopted.

The data used for each WTC estimation are the WTC observations from all data sets within the spatial and temporal influence regions, centred at the location and instant of the altimeter measurement at which the estimation is required; those ranges should equal the spatial and temporal correlation scales. However, since the period of most SI-MWR missions is in the range 100-105 minutes, the temporal influence region has been enlarged to 110 minutes for the SI-MWR dataset.

To balance the weight between the various types of observations, values of 0.5 cm have been adopted for the white noise of both MWR and GNSS-derived ZWD (Fernandes et al., 2015), whereas the associated error for each SI-MWR sensor was computed based on the standard deviation of the differences between each sensor and the values of the MWR on board the reference altimetric missions at matching points. These values are in the range 0.8 cm (for Windsat, AMSR-E and AMSR-2) and 1.2 cm (for NOAA-15, NOAA-17 and MetOp-B).

The GPD algorithm was designed to compute the WTC at ocean measurements. Initially, the computation was restricted to coastal areas, where a set of GNSS inland stations can be found. In the present implementation an estimate is obtained for every ocean point along the altimeter ground track for which the WTC computed from MWR measurements has been considered invalid. The validity of an MWR measurement is set by an MWR rejection flag (`flag_MWR_rej`) according to the following criteria

- `flag_MWR_rej` = 1 - if the `rad_surf_type` flag is 1 (land contamination)
- `flag_MWR_rej` = 2 - if the `rad_qual_interp_flag` is $\neq 0$ (only for Envisat) or if the point distance from coast is less than a given threshold ranging from 15 km for SARAL to 30 Km for all ESA missions and T/P (land contamination).
- `flag_MWR_rej` = 3 - if the `ice_flag` is 1 (ice contamination)



- flag_MWR_rej = 4 - based on statistical parameters, including median filters, function of the differences between MWR and model WTC, not only at the same measurements but also at neighbouring points (ice, land, rain or outlier detection).
- flag_MWR_rej = 5 - if the MWR WTC is $\geq 0.05\text{m}$ or $< 0.6\text{ m}$ (rain or ice contamination, or instrument failure)

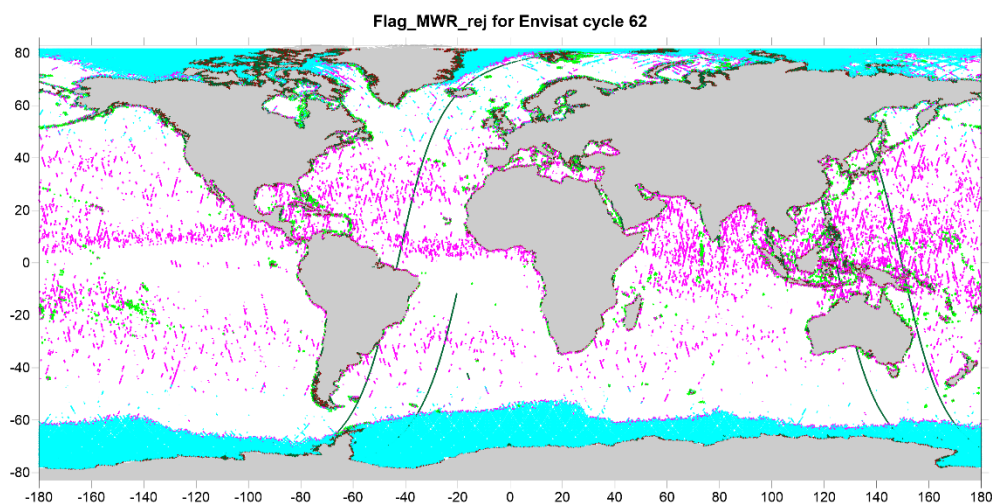
Figure 4.5 illustrates, for Envisat cycle 62 (top panel) and TOPEX/Poseidon cycle 443 (bottom panel), the points for which flag_MWR_rej is not zero, that is, the points where new values of the wet tropospheric correction are to be estimated. In addition to ocean points, to help on interpolation to higher data rates, the first land point of each track is also selected, provided it is within 50 km from the coastline (brown points in Figure 4.5). This figure demonstrates that the GPD is not merely a coastal algorithm, it is an ocean algorithm, including open-ocean, high latitudes and coastal zones.

4.4. Accuracy

Figure 4.6 illustrates the GPD formal error for Envisat cycle 62. To understand this figure, we recall that the GPD formal error is a function of the spatial and temporal distribution of the observations relative to the point of computation and also of the signal variance on the same point. The points for which there are no observations and the estimated value equals the model values adopted as first guess, were attributed a formal error of 1.5 cm. It can be observed that these points are mostly located in the polar regions, since in these regions the MWR observations are contaminated by ice.

The great majority of the points have a formal error within 1-2 cm. Considering that each output is a combination of all available observations, in the worst case, the estimation equals the first guess (model value).

Concerning the availability of valid MWR measurements, the worst cases take place when an isolated segment with all points having invalid MWR measurements occurs (usually when the track is parallel to the coastline, where a contaminated segment of several hundreds of kilometres length may occur. Due to the time difference between consecutive passes (100 minutes), in practice in the estimation of a given point only valid measurements from the same pass are used.



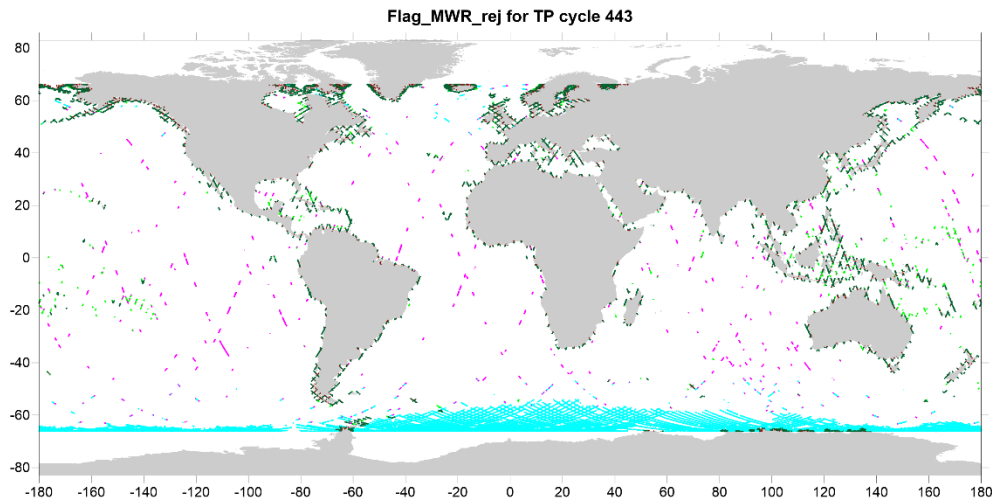


Figure 4.5 - Location of Envisat cycle 62 (top) and TP cycle 443 (bottom) points selected for the GPD computation (points with $\text{flag_MWR_rej} \neq 0$). Dark green: points with radiometer land flag set to 1; Light green: points with distance from coast less than a given threshold; Blue: points contaminated by ice; Pink: points rejected by outlier detection criteria or with the MWR WTC outside limits; Brown: land points near the coast (see text for details).

Comparing the error map with the map of the standard deviation of the WTC field shown in Figure 4.1 it can also be observed that the largest errors are also associated to regions of large field variance.

Considering the GNSS-derived path delays, various regions can be identified in Figure 4.6, e.g. around European and North American coastlines, where relatively dense networks of coastal stations can be found (c.f. Figure 4.1). However, there are many regions, particularly in the African coast, without available GNSS stations for distances of several hundreds of kilometres. In these regions the correction is solely based on valid MWR or SI-MWR measurements.

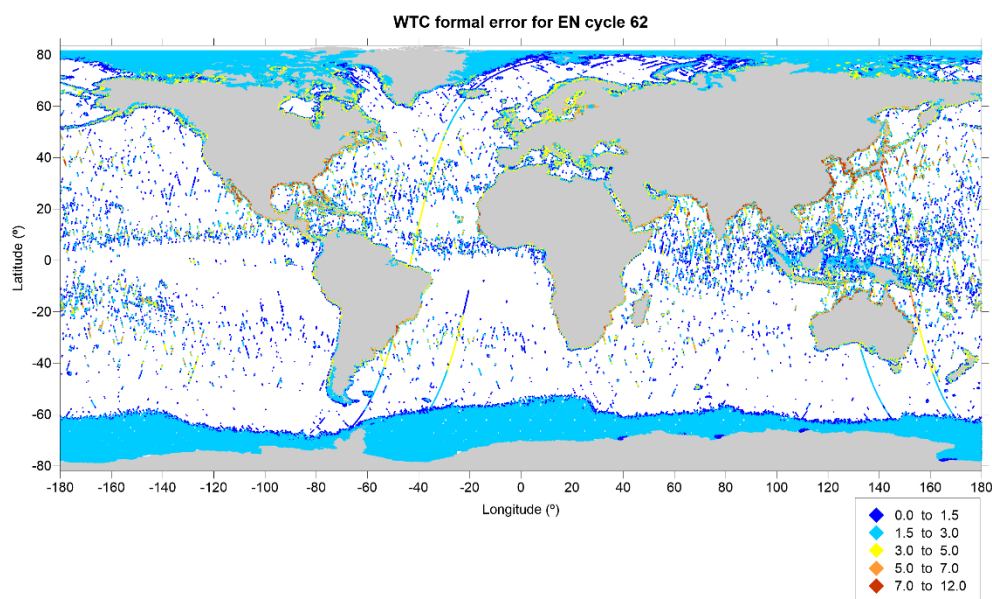


Figure 4.6 - Formal error (in cm) of the GPD wet tropospheric correction for Envisat cycle 62.



4.5. References

- Bevis M, Businger S, Chiswell S, Herring TA, Anthes RA, Rocken C, Ware RH (1994) GPS Meteorology - Mapping Zenith Wet Delays Onto Precipitable Water, *J Appl Meteorol*, 33 (3): 379-386. doi:10.1175/1520-0450
- Bosser P, Bock O, Pelon J, Thom C (2007) An improved mean-gravity model for GPS hydrostatic delay calibration, *IEEE Geosci. Rem. Sens. Letters*, 4(1): 3-7.
- Bretherton FP, Davis RE, Fandry CB (1976) A technique for objective analysis and design of oceanographic experiment applied to MODE-73, *Deep-Sea Res.*, 23: 559-582.
- Brown, S. (2010) A novel near-land radiometer wet path-delay retrieval algorithm: Application to the Jason-2/OSTM advanced microwave radiometer. *IEEE Trans. Geosci. Remote Sens*, 48, 1986-1992.
- Davis JL, Herring TA, Shapiro II, Rogers AEE, Elgered G (1995) Geodesy by radio interferometry: effects of atmospheric modelling errors on estimates of baseline length. *Radio Sci* 20(6):1593-1607.
- Dee, D.P., Uppala, S.M., Simmons, A.J., Berrisford, P., Poli, P., Kobayashi, S., Andrae, U., Balmaseda, M.A., Balsamo, G., Bauer, P., et al (2011) The ERA-Interim reanalysis: Configuration and performance of the data assimilation system. *Q. J. R. Meteorol. Soc.*, 137, 553-597. ECMWF (2009) <http://www.ecmwf.int/products/catalogue/pseta.html>
- Fernandes, M.J.; Nunes, A.L.; Lázaro, C., (2013) Analysis and Inter-Calibration of Wet Path Delay Datasets to Compute the Wet Tropospheric Correction for CryoSat-2 over Ocean. *Remote Sens*. 2013, 5(10), 4977-5005, <http://www.mdpi.com/2072-4292/5/10/4977>
- Fernandes M. Joana, Clara Lázaro, Michaël Ablain, Nelson Pires.(2015) Improved wet path delays for all ESA and reference altimetric missions, *Remote Sensing of Environment*, Volume 169, November 2015, Pages 50-74, ISSN 0034-4257, <http://dx.doi.org/10.1016/j.rse.2015.07.023>.
- Fernandes MJ, Lázaro C, Nunes AL, Pires N, Bastos L, Mendes VB (2010) GNSS-derived Path Delay: an approach to compute the wet tropospheric correction for coastal altimetry. *IEEE Geosci. Rem. Sens Lett.*, 7(3): 596-600.
- Fernandes MJ, Pires N, Lázaro C, Nunes AL (2012) Tropospheric Delays from GNSS for Application in Coastal Altimetry. *Adv Space Res*. doi:10.1016/j.asr.2012.04.025. (Accepted for publication in ASR Special Issue: Altimetry Calibration)
- Kouba J (2008) Implementation and testing of the gridded Vienna Mapping Function 1 (VMF1), *Journal of Geodesy*, 82:193-205. doi:10.1007/s00190-007-0170-0
- Leeuwenburgh O (2000) Covariance modelling for merging of multi-sensor ocean surface data, *Methods and Applications of Inversion*, *Lect. Notes Earth Sci.*, vol. 92.
- Mendes VB, Prates G, Santos L, Langley RB (2000) An evaluation of the accuracy of models of the determination of the weighted mean temperature of the atmosphere. In: *Proceedings of "ION 2000 National Technical Meeting"*, Anaheim, CA.
- Miller M, Buizza R, Haseler J, Hortal M, Janessen P, Untch A (2010) Increased resolution in the ECMWF deterministic and ensemble prediction systems. *ECMWF Newsletter* 124: 10-16.
- Scharroo, R., Lillibridge, J.L., Smith, W.H.F., Schrama, E.J.O. (2004) Cross-calibration and long-term monitoring of the microwave radiometers of ERS, TOPEX, GFO, Jason and Envisat. *Marine Geodesy.*, 27, 279-297.
- Schüler J (2001) On ground-based GPS tropospheric delay estimation, PhD Dissertation, Universität der Bundeswehr, München.
- Wentz, F., j. (2013) SSM/I Version-7 Calibration Report, RSS Technical Report 011012, Remote Sensing Systems, January 11, 2013.



5. ATBD-3: To compute the sea state biases

5.1. Selected altimeter standards

Name	Description	Mission applicability
Sea State Bias No-parametric solutions (Labroue 2007 ;Tran 2010; Tran 2012 ; Tran 2015)	This correction is interpolated on 1Hz measurements from a 2-dimensional table which contains: <ul style="list-style-type: none"> • altimetric Ku waves • altimetric Ku wind 	ERS-2, EnviSat, TOPEX/Poseidon, Jason-1, Jason-2, SARAL/AltiKa, CryoSat-2

5.2. Function

To compute the sea state bias in the main and in the auxiliary frequency bands. The sea state bias is the difference between the apparent sea level as "seen" by an altimeter and the actual mean sea level.

5.3. Algorithm Definition

5.3.1. Input data

- Significant waveheight:
 - Significant waveheight (main band)
 - Associated validity flag
- Wind speed:
 - Wind speed corrected for atmospheric attenuation (W)
- Sea state bias table (SAD)

5.3.2. Output data

- Sea state bias in main and in auxiliary bands

5.3.3. Mathematical statement

The SSB is bi-linearly interpolated from a SAD table that is provided as a function of significant waveheight (main band) and of wind speed, with same values for the main and the auxiliary bands.

5.4. Accuracy

The underlying physics of the sea state bias is not completely understood. The estimated global RMS accuracy is about 2 cm (Gaspar and Florens, 1998).



5.5. References

- Gaspar, P., and J.P. Florens, 1998 : Estimation of the sea state bias in radar altimeter measurements of sea level : Results from a new nonparametric method.J. Geophys. Res, Vol 103, NO. C8, 15803-15814.
- Gaspar, P., and F. Ogor, 1996: Estimation and analysis of the Sea State Bias of the new ERS-1 and ERS-2 altimetric data (OPR version 6). Report of task 2 of IFREMER Contract n° 96/2.246002/C.



6. ATBD-4: To compute ionosphere correction derived from Nic09 model

6.1. Selected altimeter standards

Name	Description	Mission applicability
Ionosphere correction derived from Nic09 model	The NICO09 model is a 5-dimensional climatology that can be interpolated in space, time, and GTEC to obtain an estimate for the TEC at any location on Earth and at any time. It is described in Scharroo et al, "A GPS based climatology for the total electron content in the ionosphere", JGR.	ERS-1

6.2. Function

To compute the Nic09 ionosphere correction (based on a GPS climatology for the total electron content in the ionosphere) of the sea surface topography at the altimeter time tag and location.

6.3. Algorithm Definition

6.3.1. Input data

- The NICO09 ionosphere climatology, netcdf File : ftp://ibis.grdl.noaa.gov/pub/remko/nic09/nic09_clim.nc which contains the global mean total electron content by months, hours, latitude and longitudes .
- The Global mean total election content from combined sources: ftp://ibis.grdl.noaa.gov/pub/remko/nic09/nic09_gtec.nc which contains the global mean total electron content versus time.
- Altimeter location : 1-Hz altimeter time tag, latitude, longitude

6.3.2. Output data

- The ionospheric correction derived from the Nic09 climatology

6.3.3. Mathematical statement

The TEC varies linearly with GTEC, and the intercept and slope of the linear variation depends on time of day as well as the month of the year. Equally, these parameters depend on the location as well. This results eventually in a 5-dimensional climatology that can be interpolated in space, time, and GTEC to obtain an estimate for the TEC at any location on Earth and at any time for which we know the GTEC. The five dimensions, illustrated in Figure 6.1, are as follows:

- **Longitude:**



The same longitude nodes as the GIM TEC maps are used (spaced 5° apart). The 73 grid nodes in those maps range from 180° W to 180° E, where the latter is a copy of the former. The climatological solution at these points is the same as well.

- **Latitude:**

Again, the same latitude nodes as the GIM TEC maps are used (spaced 2.5° apart). The GIM maps do not include the polar latitudes 90° S and 90° N. To obtain a truly global solution we fill in these latitudes with the average of the solutions along the 87.5° S and 87.5° N parallels, respectively. We thus have 73 nodes.

- **Month:**

Twelve monthly vertices determine a piece-wise linear function. The year is divided into twelve equal periods and a grid node is placed in the middle of each period. Each TEC observation falling in between those nodes contributes to the nodes on either side of the epoch. This means that the monthly solutions have to be solved simultaneously. The placement of the nodes in the middle of the monthly periods—rather than at the beginning—is not totally arbitrary; the monthly grids used in the IRI models also refer to the month centres. In case of IRI, however, the months are calendar months, rather than the equally spaced periods in our solution.

- **Hour:**

Twelve 2-hourly vertices determine another piece-wise linear function. These vertices are at even hours UTC and coincide with the epochs of the “synchronised” GIM TEC maps

- **GTEC:**

Two levels of GTEC are solved for a low level of solar activity corresponding to 10 TECU (1 TECU=10¹⁶ electrons/m²), and a high level corresponding to 70 TECU. This is equivalent to estimating an offset and a slope of the linear variations discussed above. Each TEC observation contributes proportionally to both parameter estimates depending on the GTEC at that moment. A weighted linear least-squares solution can be determined for each location and each even hour. All GIM TEC observations at that location and hour are fitted in a manner similar to the equation 6.1 below, replacing a and b by the equivalent expressions in terms of a GTEC at 10 and 70 TECU.

$$\text{TEC}(l;f;m;h; t) = a(l;f;m;h)+b(l;f;m;h)*\text{GTEC}(t) \quad \text{Eq 6.2}$$

where “l” is the longitude, “f” is the latitude, “m” is the month, “h” is the hour and “t” are the two levels of GTEC considered

In this way at each of the 72x71 locations 12 independent 2-hourly fits determined by 12x2 parameters are solved for. The root mean square (RMS) fit of each of those models is stored, resulting in 12 global maps (one per each 2-hourly period). If we were to use the original TEC maps (at mixed odd and even hours) as input we would have to estimate the 2-hourly, longitudinal and latitudinal dimensions simultaneously, leading to one set of 72x71x12x12x2 parameters, which would require excessive amounts of memory and time to compute. Figure 6.2 illustrates the climatology by mapping, in the foreground, 24 global TEC predictions during high solar activity. From top to bottom the daily progression of the Appleton anomaly along the geomagnetic equator can be followed. The Appleton or equatorial anomaly denotes regions of enhanced plasma density some 10° to 15° in latitude north and south of the dip equator, occurring from pre-noon through midnight hours. [H. Lühr et al, 2003²]”From left to right the monthly solutions highlight seasonal variations such as the increase of TEC during the respective hemispherical summers.

² <http://onlinelibrary.wiley.com/doi/10.1029/2003GL017407/full>

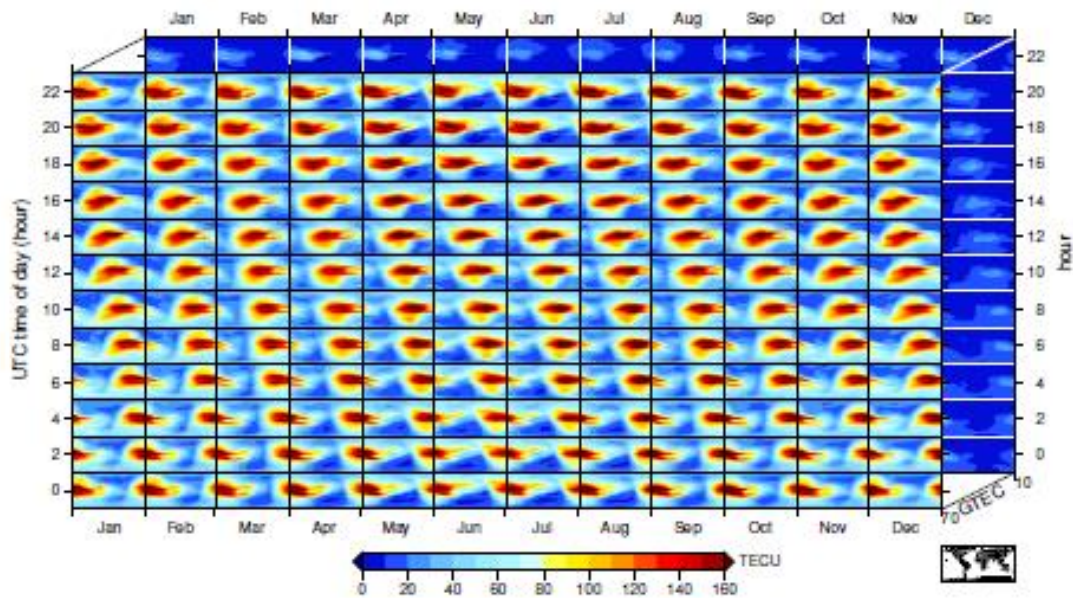


Figure 6.1- Illustration of the 5-dimensional TEC climatology. The foreground shows the monthly and 2-hourly global grids at times of high solar activity (GTEC is 70 TECU). In the background are the solutions for low solar activity (GTEC is 10 TECU).

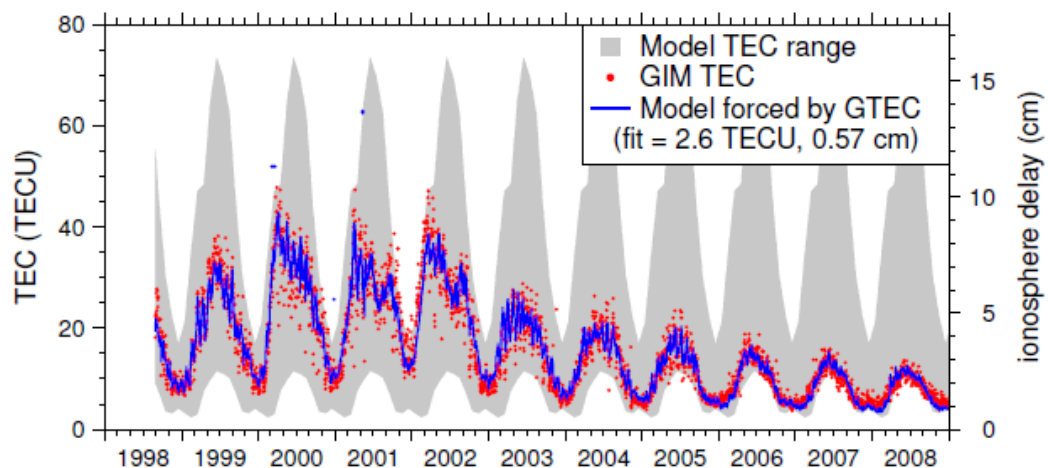


Figure 6.2 - The red dots denote the TEC near Greenwich at 20:00 UTC according to JPL GIM. The blue line is the climatological fit. The residuals have an RMS of 2.6 TECU. The grey region represents the model's TEC range for GTEC values between 10 and 70.

6.4. Accuracy

In **Figure 6.3** the dual-frequency altimeter measurements of TOPEX, Jason-1 and Envisat are compared with the interpolated GIM maps and the NIC09 and IRI2007 climatologies along two long passes across the Atlantic Ocean. Although GIM does not provide a perfect match, it follows the main features in the along-track TEC to within 20 TECU (4.3 cm of equivalent Ku-band delay), even during the high solar activity of 2002. While NIC09 is not expected to perform better than GIM (Remko and Smith, 2010; WP2400 SL_cci phase I validation report, 2012; RRDP SL_cci phase I, 2012), there are the occasional passes for which NIC09 actually comes closer to the measurements.



The RMS error in Ku-band path delay of less than 10 TECU (2 cm) is typical for this period (see also **Figure 6.4**) and is acceptable for most ocean applications. IRI2007 performs significantly worse, generally underestimating the TEC around the equator and producing more erratic results towards the poles. A plot of the time series of the RMS difference between the models and altimeter measurements (**Figure 6.4**) affirms the relative accuracy of each of the models and also suggests that the RMS errors in the models are more or less proportional to the TEC itself. Indeed, in **Figure 6.3**, the spread of the differences between models and measurements increases more or less linearly with increasing TEC. A regression analysis demonstrates that the RMS error of the GIM TEC (or ionospheric delay) is approximately 14%, NIC09 18%, and IRI2007 35%. That means that for periods where the IRI2007 model is the only alternative, NIC09 potentially reduces the error variance in the ionospheric delay by as much as 70%.

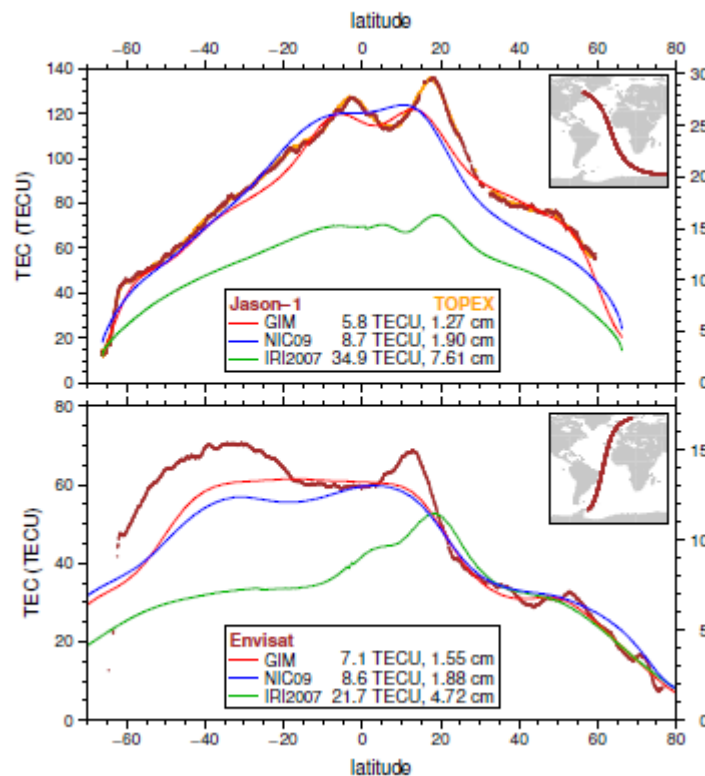


Figure 6.3 - Examples of model results and measurements of TEC (left ordinate) and Ku-band ionosphere delay (right ordinate) along two long ocean-only passes across the Atlantic. Dots indicate dual-frequency altimeter measurements. The model results from GIM, NIC09 and IRI2007 are shown as lines. The numbers in the legends indicate the RMS difference between the measurements and models. Top: TOPEX and Jason-1, 6 Mar 2002 around 15:00 UTC. Bottom: Envisat, 20 Dec 2002 around 12:00 UTC.

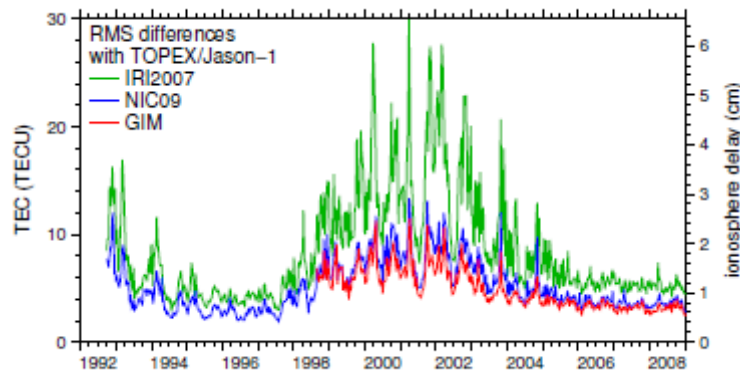


Figure 6.4 - Global RMS difference between the results from various models and the dual-frequency altimeter measurements of TOPEX and Jason-1.

6.5. References

- RRDP SL_cci phase I, 2012. Ionospheric models comparison: NIC09 versus GIM. http://www.esa-sealevel-cci.org/webfm_send/163
- R.Scharroo, W,Smith. A GPS based climatology for the total electron content in the ionosphere. JOURNAL OF GEOPHYSICAL RESEARCH, VOL. 115, 2010, DOI:10.1029/2009JA014719, 2010.
- WP2400 SL_cci phase I validation report, 2012. Ionosphere correction. http://www.esa-sealevel-cci.org/webfm_send/178



7. ATBD-5: To compute the high frequency fluctuations

7.1. Selected altimeter standards

Name	Description	Mission applicability
Dynamical atmospheric correction derived from ERA-interim model	<p>The DAC correction is a combination of high frequencies of a barotropic model forced by pressure and wind (MOG2D model: <i>Carrère and Lyard 2003</i>; <i>SWT New Orleans 2002</i>) and the low frequencies of the IB.</p> <p>In the context of the T/P and Jason-1&2 reference missions, the high frequencies have been defined to be the periods lower than 20 days, which exactly corresponds to the Nyquist frequency of these altimeters' sampling.</p>	All missions

7.2. Function

To compute the high frequency fluctuations of the sea surface topography at the altimeter time tag and location from MOG2D model based on the ERA-Interim reanalysis computed by ECMWF.

7.3. Algorithm definition

7.3.1. Input data

- Datation:
 - 1-Hz altimeter time tag
- Location:
 - Latitude of the measurement (1 Hz)
 - Longitude of the measurement (1 Hz)
- MOG2D data: sum of the high frequency variability of the sea surface height and of the low frequency part of the inverted barometer effect (DAD) as computed in ERA-Interim.
- The data consists of two data files, 6 hours apart, surrounding the time of measurement (each file containing the parameter given on regular grid).

7.3.2. Output data

- High frequency fluctuations of the sea surface topography (sum of the high frequency variability of the sea surface height and of the low frequency part of the inverted barometer effect) at the altimeter measurement time tag and location

7.3.3. Mathematical statement

The T/P and Jason altimeters (10-day repeat cycle) deliver very accurate data sets (within 2 centimeter global error for T/P). However for mesoscale circulation applications and satellite



calibration campaigns, the HF ocean signal (periods less than 20 days for T/P), is aliased into the low frequency band (LF; periods larger than 20 days for T/P), and needs to be corrected from independent models at centimetric accuracy. The present HF tidal corrections have mainly reached this requirement, through the high resolution hydrodynamic models. In contrast, the ocean response to meteorological forcing results poorly accounted if only the inverted barometer correction (IB) is applied. The MOG2D-G models the high frequency (HF) atmospheric forced variability of the global ocean with unprecedented accuracy. This hydrodynamic finite element (FE) model provides a global simulation of the ocean response to atmospheric wind and pressure forcing. MOG2D parameters (sum of the high frequency variability of the sea surface height and of the low frequency part of the inverted barometer effect) at the altimeter measurement are obtained by linear interpolation in time between two consecutive (6 hours apart) MOG2D model data files, and by bilinear interpolation in space from the four nearby model grid values.

- The longitude of the altimeter measurement : Alt_Lon_Mean
- The latitude of the altimeter measurement : Alt_Lat_Mean
- The grid step in longitude : Lon_Step
- The grid step in latitude : Lat_Step
- The longitude of the first grid point : Lon-First
- The latitude of the first grid point : Lat_First
- The number of grid points in longitude : Nb_Lon
- The number of grid points in latitude : Nb_Lat
- The cycling value in longitude : 360
- The cycling value in latitude : 0
- The truncation flag in longitude : 0
- The truncation flag in latitude : 0
- The indexes of the four grid points surrounding the measurement point: LL(lower Left), LR (lower right), UL (upper left), UR (upper right)
- The weights of these four points:
- The execution status

$$\left. \begin{aligned} V_{LL}(i, j) &= MOG2D(i, j(lon_L(i))) \\ V_{LR}(i, j) &= MOG2D(i, j(lon_R(i))) \\ V_{UL}(i, j) &= MOG2D(i, j(lat_L(i))) \\ V_{UR}(i, j) &= MOG2D(i, j(lat_U(i))) \end{aligned} \right\} \text{are the four nearby model values}$$

- The parameter interpolated in space at altimeter measurement MOG2D_Int_Space
- The number of valid cell points used by the interpolation (unused)
- The execution status



7.4. Accuracy

The Dynamic Atmospheric Correction (DAC) is based on a global barotropic model (MOG2D), which has inherent errors due to the physics approximations, the grid size (ranging from 400 km in deep ocean to 20 km in coastal, shallow areas.), the forcing fields, the bathymetry errors, etc. Model outputs have been extensively compared to in situ data (tidal gauge, noted TGs; Carrère et Lyard 2003; Carrère, 2013): the model represents about 80 % of the high frequency variability and it allows reducing the TG variance by more than 50% if compared to the static IB; at low latitudes (between +/- 30°) the model is less efficient (gain of 10-20%) due to the dominance of the baroclinic signal, however signal is very weak in these regions. The residual variance of the temporal series corrected from the DAC correction, gives an estimation of the global error of this component, including: modelling errors (bathymetry, mesh resolution, forcing errors, etc.) and omissions errors, due to the lack of baroclinic physics for example. This global error is less than 10 % at high latitudes, and between 40-80 % at low latitudes; if looking at cm², the residual variance is lower than 2 cm² in the intertropical region, where the variability at high frequencies is very weak, and about 5-10 cm² near the coasts (locally more than 100 cm²), where the high frequency variability is strong. Concerning barotropic velocities, the error distribution is mainly localized in coastal margin and in cape-like areas; in deeper regions this error is negligible.

7.5. References

Loren Carrere and Florent Lyard, "Modeling the barotropic response of the global ocean to atmospheric wind and pressure forcing - comparison with observations", *Geophysical Research Letters*, Vol. 30, NO 6, 1275, doi:10.1029/2002GL016473, 2003



8. ATBD-6: Dry troposphere corrections derived from ERA-interim pressure fields

8.1. Selected altimeter standards

Name	Description	Mission applicability
Dry troposphere derived from ERA-interim pressure fields.	The dry troposphere (DT) is computed from ERA Interim pressure fields.	All missions

8.2. Function

To compute at the altimeter time tag and location the dry tropospheric corrections (DTCs) due to gases of the troposphere from ERA Interim pressure fields to which a model of S1 and S2 atmospheric pressure tides is added.

8.3. Algorithm definition

8.3.1. Input data

- Datation:
 - 1-Hz altimeter time tag
- Location:
 - Latitude of the measurement (1 Hz)
 - Longitude of the measurement (1 Hz)
- Surface type:
 - Surface type (“open ocean or semi-enclosed seas”, “enclosed seas or lakes”, “continental ice”, or “land”)
- Meteorological data (DAD):
 - Meteorological data: surface pressure and mean sea surface pressure. For each of these 2 parameters, the data consist of two data files, 6 hours apart, bracketing the time of measurement (each file, excepted the mean sea surface pressure, contains the parameter given on the so-called Gaussian grid (quasi regular in latitude, non-regular in longitude).
 - Table providing the latitudes of the model grid points
 - Table providing the number of grid points in longitude for each model latitude
- Climatological pressure files (SAD)
 - The data consists of four data files, corresponding to 0h, 6h, 12h and 18h. Each file contains the climatological pressure referenced to the sea on a Cartesian grid, for each of the twelve months of the year.
- S1 and S2 tide grids of monthly means of global amplitude and phase
- Processing parameters (SAD)



8.3.2. Output data

- Dry tropospheric correction: δh_{dry}

8.3.3. Mathematical statement

The surface pressure and the mean sea surface pressure at the altimeter measurement are obtained by linear interpolation in time between two consecutive (6 hours apart) ERA-Interim model data files, and by bilinear interpolation in space from the four nearby model grid values (excepted for the mean sea surface pressure). The ERA-Interim model grid is quasi regular in latitude and non-regular in longitude (the number of grid points in longitude increases towards lower latitudes). If the surface type of the altimeter measurement is set to “open ocean or semi-enclosed seas”, only grid points having negative altitude are used in the interpolation (to avoid wrong tropospheric correction to be computed over ocean due to a grid point over high land altitude). If no such grid points with negative altitude are found, then the four grid points having positive altitude are used. If the altimeter measurement is set to “enclosed seas or lakes”, “continental ice”, or “land”, all grid points are used in the interpolation, whatever their altitude is.

The climatological S1 and S2 pressure (0h, 6h, 12h and 18h for each month) is then removed from the surface pressure, to correct from the aliasing of these signals due to the 6-hours sampling of the meteorological fields.

Finally, the dry tropospheric correction is derived from the surface pressure (climatological pressure removed) to which a model of S1 and S2 pressure variability (R D Ray and R M Ponte, 2003) is added.

Hereafter are detailed the mathematical statement used at Météo-France to compute the surface pressure map and the wet tropospheric correction map. The input data for computing these maps at Météo-France are the model surface pressure, and the specific humidity and temperature profiles from the vertical levels of the ERA-Interim model.

Definitions of the refractive index and of the dry tropospheric corrections

The excess propagation path, also called path delay, induced by the neutral gases of the atmosphere between the backscattering surface and the satellite is given by:

$$\delta h = \int_{H_{\text{surf}}}^{H_{\text{sat}}} (n(z) - 1) dz \quad \text{Eq 8.1}$$

where $n(z)$ is the index of refraction of air, H_{surf} and H_{sat} are respectively the altitudes of the surface and of the satellite above mean sea level.

The index of refraction is conveniently expressed in terms of the refractivity $N(z)$, defined as:

$$10^{-6} N(z) = n(z) - 1 \quad \text{Eq 8.2}$$

$N(z)$ is given by Bean and Dutton (1966):



$$N(z) = 77.6 \frac{P_d}{T} + 72 \frac{e}{T} + 3.75 \cdot 10^5 \frac{e}{T^2} \quad \text{Eq 8.3}$$

where P_d is the partial pressure of dry air in hPa (1 hPa = 100 Pa), e is the partial pressure of water vapor in hPa, and T is temperature in K.

As the partial pressure of dry air is not easily measured, it is desirable to obtain an expression function of the total pressure of air. For deriving it, we have to consider that the dry air and the water vapor are ideal gases, i.e., they obey to the Mariotte-Gay Lussac law:

$$\text{For dry air: } \frac{P_d}{\rho_d} = \frac{RT}{M_d} \quad \text{Eq 8.4}$$

$$\text{For water vapor: } \frac{e}{\rho_w} = \frac{RT}{M_w} \quad \text{Eq 8.5}$$

where ρ_d and ρ_w are the volumic masses of dry air and water vapor respectively, M_d and M_w are the molar masses of dry air ($28.9644 \cdot 10^{-3}$ kg) and water vapor ($18.0153 \cdot 10^{-3}$ kg) respectively, R is the universal gas constant ($8.31434 \text{ J.mole}^{-1}.\text{K}^{-1}$).

Combining Eq 8.4, Eq 8.5 and Eq 8.3 leads to:

$$N(z) = 77.6 R \frac{\rho_d}{M_d} + 72 R \frac{\rho_w}{M_w} + 3.75 \cdot 10^5 \frac{e}{T^2} \quad \text{Eq 8.6}$$

The volumic mass of wet air is the sum of the volumic masses of dry air and water vapor: $\rho = \rho_d + \rho_w$ Eq 8.7

Introducing the volumic mass of wet air given by Eq 8.7 into Eq 8.6 leads to:

$$N(z) = 77.6 R \frac{\rho}{M_d} + (72 - 77.6 \frac{M_w}{M_d}) R \frac{\rho_w}{M_w} + 3.75 \cdot 10^5 \frac{e}{T^2} \quad \text{Eq 8.8}$$

Reintroducing Eq 8.5 into Eq 8.8 leads to the final expression of refractivity $N(z)$:

$$N(z) = 77.6 R \frac{\rho}{M_d} + (72 - 77.6 \frac{M_w}{M_d}) \frac{e}{T} + 3.75 \cdot 10^5 \frac{e}{T^2} \quad \text{Eq 8.9}$$

Combining this expression with Eq 8.1 and Eq 8.2 leads to the following equation for δh :

$$\delta h = 77.6 \cdot 10^{-6} \frac{R}{M_d} \int_{H_{\text{surf}}}^{H_{\text{sat}}} \rho dz + (72 - 77.6 \frac{M_w}{M_d}) \cdot 10^{-6} \int_{H_{\text{surf}}}^{H_{\text{sat}}} \frac{e}{T} dz + 3.75 \cdot 10^{-1} \int_{H_{\text{surf}}}^{H_{\text{sat}}} \frac{e}{T^2} dz \quad \text{Eq 8.10}$$



The first term is called the dry tropospheric correction δh_{dry} :

$$\delta h_{\text{dry}} = 77.6 \cdot 10^{-6} \frac{R}{M_d} \int_{H_{\text{surf}}}^{H_{\text{sat}}} \rho \, dz \quad \text{Eq 8.11}$$

The sum of the two remaining terms is called the wet tropospheric correction

$$\delta h_{\text{wet}} = (72 - 77.6 \frac{M_w}{M_d}) 10^{-6} \int_{H_{\text{surf}}}^{H_{\text{sat}}} \frac{e}{T} \, dz + 3.75 \cdot 10^{-1} \int_{H_{\text{surf}}}^{H_{\text{sat}}} \frac{e}{T^2} \, dz \quad \text{Eq 8.12}$$

Introducing the numerical values for M_d and M_w into Eq 8.12, and multiplying δh_{wet} by -1 to get a negative quantity to be added to the altimeter range, leads to the following equation for δh_{wet} in m:

$$\delta h_{\text{wet}} = -23.7 \cdot 10^{-6} \int_{H_{\text{surf}}}^{H_{\text{sat}}} \frac{e}{T} \, dz - 3.75 \cdot 10^{-1} \int_{H_{\text{surf}}}^{H_{\text{sat}}} \frac{e}{T^2} \, dz \quad \text{Eq 8.13}$$

Calculation of the dry tropospheric correction as function of the surface pressure

It is commonly assumed that the atmosphere is in hydrostatic equilibrium, i.e. g being the acceleration due to gravity:

$$\frac{dP}{dz} = -\rho g \quad \text{Eq 8.14}$$

Combining Eq 8.11 and Eq 8.14 leads to the following equation for δh_{dry} , where P_{surf} is the atmospheric pressure at the ground surface:

$$\delta h_{\text{dry}} = 77.6 \cdot 10^{-6} \frac{R}{M_d} \int_0^{P_{\text{surf}}} \frac{1}{g} \, dP \quad \text{Eq 8.15}$$

The dry tropospheric correction map given by Météo-France is computed from Eq 8.15.

The acceleration of gravity is a function of latitude and altitude. This function can be modelled by:

$$g = g_0 \cdot [1 - 0.0026 \cos(2\phi) - 0.00031z] \quad \text{Eq 8.16}$$

where ϕ is the latitude, z is altitude in km, and $g_0 = 9.80665 \text{ m/s}^2$

The variation of g with altitude is small and can be neglected by considering a mean value for $g = 9.783 \text{ m/s}^2$ constant with altitude. This leads to the final expression for δh_{dry} :

$$\delta h_{\text{dry}} = -2.277 P_{\text{surf}} \cdot [1 + 0.0026 \cos(2\phi)] \quad \text{Eq 8.17}$$



Eq 8.17 is the expression obtained by Saastamoinen (1972), where P_{surf} is in hPa, and δh_{dry} is in mm and is set here with a negative sign to be added to the altimeter range. Computing the dry tropospheric correction from Eq 8.15 instead of from Eq 8.17 (i.e., taking into account the variation of g with altitude, as given by Eq 8.16), leads to differences below the 1-mm level in dry tropospheric correction (below the 0.5-mm level for latitudes less than 50°).

Note In this algorithm, the dry tropospheric correction will be computed as described in Eq 8.17 but using a surface pressure which is the interpolated surface pressure P_{surf} from which the climatological pressure is removed (over the ocean only) and to which a model of S1 and S2 waves pressure variability (R D Ray and R M Ponte, 2003) is added.

8.4. Accuracy

The accuracy of the dry tropospheric correction primarily depends on the accuracy of the surface pressure [Saastamoinen, 1972]. The best accuracy for surface pressure is achieved for analyzed fields. Typical errors vary from 1 hPa in northern Atlantic to more than 10 hPa in southern Pacific [Ray & Ponte, 2003]. A 1 hPa error on pressure translates to a 2 mm error on the dry tropospheric correction. The error introduced by space and time interpolation under the satellite track is probably small compared with the intrinsic inaccuracy of the surface pressure [Ray & Ponte, 2003]. For land surfaces, additional error is induced by the calculation of the surface pressure from the upper level pressure, due to assumptions on the mean virtual temperature of the atmospheric layer between the surface and the first upper level above the ground surface, and due to inaccurate knowledge of the TerrainBase digital elevation model (DEM) used for computing the altitude of the grid points above mean sea level. This additional error may be as large as the intrinsic error of the upper level pressure [Ray & Ponte, 2003].

8.5. References

- Bean, B. R., and E. J. Dutton, Radio Meteorology, U.S. NBS Monogr., 92, March 1966.
- Saastamoinen, J., 1972: Atmospheric correction for the troposphere and stratosphere in radio ranging of satellites, Geophys. Monogr., 15, American Geophysical Union, Washington D.C.
- R D Ray and R M Ponte, Barometric tides from ECMWF operational analyses, Annales Geophysicae, 21: 1897-1910, 2003.



9. ATBD-7: To compute ocean tide height (including long period equilibrium ocean tide) and load tide height

The geocentric (elastic) ocean tide is the sum of the ocean tide and the load tide. It is a major contributor to sea level variability and it is observed by altimeters on board satellites.

9.1. Selected altimeter standards

Name	Description	Mission applicability
FES2014 tide model	The tide model computes the tide correction at satellites location and date using FES2014 wave tide files of amplitude and phase.	All missions

9.2. Function

- To compute the ocean tide from the FES2014 harmonic components algorithm (using FES2014 model), using the diurnal and semidiurnal components as well as some non linear and long-period ones. To add the height of the equilibrium long period ocean tide. The ocean tide height does not include the load tide height.
- To provide the ocean tide (including long period ocean tide) in output.
- To compute the height of the tidal loading induced by the ocean tide from GOT4v8ac harmonic components.
- To provide the load tide in output. To add the ocean tide (including long period ocean tide) and the load tide to compute the geocentric (elastic) ocean tide.

9.3. Algorithm Definition

9.3.1. Input data

- Datation:
 - Altimeter time tag
- Location:
 - Latitude of the measurement
 - Longitude of the measurement
- Height of the equilibrium long period ocean tide: long period tides are gravitational tides, typically with amplitudes of a few centimeters or less and periods longer than a day, generated by changes in the Earth's orientation relative to the Sun and Moon. The equilibrium tide height is defined to be proportional to the gradient of the tide potential, assuming a rigid spheric Earth covered by a thin water layer with no inertia, nor viscosity.
- Harmonic coefficients maps of the principal tidal waves (SAD)
- Load tide harmonic coefficients maps of the principal tidal waves (SAD)



- The frequencies and the phases at 0h on 1/1/1900 of five astronomical variables, respectively the mean longitude of the moon, the mean longitude of the sun, the mean longitude of the lunar perigee, the negative of the mean longitude of the lunar ascending node and the mean longitude of the solar perigee
- The frequencies of the 34 tidal waves
- The admittance parameters

9.3.2. Output data

- Ocean tide height including long period ocean tide (solution 1 = FES2014 harmonic components)
- Height of the tidal loading (solution 1 = GOT4.8ac harmonic components)

9.3.3. Mathematical statement

- The height of the ocean tide is the sum of N tidal constituents h_i (Schureman, 1958):

$$h_i = F_i \cdot [A_i(\phi, \mu) \cdot \cos(\psi_i) + B_i(\phi, \mu) \cdot \sin(\psi_i)] \quad (i=1, N) \quad \text{Eq 9.1}$$

with: $\psi_i = \sigma_i \cdot t + X_i + U_i$

F_i is the tidal coefficient of amplitude nodal correction (depends only on the altimeter time)

U_i is the tidal phase nodal correction (depends only on the altimeter time)

X_i is the tidal astronomical argument (depends only on the altimeter time)

σ_i is the tidal frequency

t , ϕ and μ are respectively the altimeter time tag, latitude and longitude

$A_i(\phi, \mu)$ and $B_i(\phi, \mu)$ are harmonic coefficients bi-linearly interpolated at the altimeter location (ϕ, μ) from the input harmonic coefficients map given by the GOT4.8 model (Ray, 1999). Harmonic coefficients A and B are tidal amplitude x $\cos(\text{phase})$ and tidal amplitude x $\sin(\text{phase})$ respectively.

- The height of the tidal loading is the sum of N constituents h_i :

$$h_i = F_i \cdot [C_i(\phi, \mu) \cdot \cos(\psi_i) + D_i(\phi, \mu) \cdot \sin(\psi_i)] \quad (i=1, N) \quad \text{Eq 9.2}$$

$C_i(\phi, \mu)$ and $D_i(\phi, \mu)$ are harmonic coefficients bi-linearly interpolated at the altimeter location (ϕ, μ) from the input harmonic coefficients map. This map has been computed from Ray (1999). $N = 26$ tidal constituents were used. Among these 26 tidal constituents, 8 principal ones were given in input amplitudes and phases maps, the 18 remaining ones were computed by admittance from the principal constituents 1 to 8, using admittance coefficients.

Two additional principal waves (S1 and M4) are taken into account, leading thus to a total number of 28 components.

- The height of the geocentric (elastic) ocean tide height is the sum of the height of the ocean tide, including the height of the equilibrium long period ocean tide (input of the algorithm), and the height of the tidal loading.



9.4. Accuracy

A typical value for deep ocean tide model error is a 1 cm error (Lyard et al. 2006; Ray, 2011; Carrère et al, 2012; Cancet et al.2012). This error will likely be reduced while improving the in situ comparison dataset (work being done by R. Ray, personal communication 2013). In shallow water this error is higher due to higher modelling and omission errors: the modelling error includes bathymetry error, mesh resolution, and hydrodynamic approximations error, and the omission error is due to the lack of non-linear waves in most of models. The global rms difference with a 179-shallow-waters database is about 10 cm (Ray, 2011), but it can reach several tens of cm if compared to a more complete and coastal database (Cancet et al, 2012; Carrère et al. 2012): between 18-36 cm error for M2 wave if compared to a coastal dataset, and between 20-50 cm for a shelf database (extended dataset if compared to R. Ray's one).

9.5. References

Cancet, M. and J. Lamouroux (2012), Modèle de marée FES2012 - tâche 4, NOV-3918-NT-12304_v2.0.pdf, 10/2012.

Carrère L. and Lyard F., Modelling the barotropic response of the global ocean to atmospheric wind and pressure forcing - comparisons with observations , GRL, 30 (6), pp 1275, 2003.

Carrère L., F. Lyard, M. Cancet, A. Guillot, L. Roblou (2012), FES 2012: a new global tidal model taking advantage of nearly 20 years of altimetry, Proceedings of 20 years of Altimetry, Venice 2012.

Carrère L, S Dupuy (2013), Rapport annuel SALP-DAC pour 2012, SALP-RP-MA-EA-22182-CLS-NT-13-032.

Lyard, F., et al. (2006), Modeling the global ocean tides: a modern insight from FES2004, Ocean Dynamics, 56, 394-415.

Ray, R.D. (2013), Precise comparisons of bottom-pressure and altimetric ocean tides, J. Geophys. Res. Oceans, 118, 4570-4584, doi:10.1002/jgrc.20336.

Shum, C.K. et al. (1997), Accuracy assessment of recent ocean tide models, JGR, 102 (C11).

Schureman, P. (1958), Manual of harmonic analysis and prediction of tides, US Department of Commerce, Special Publication No. 98.



10. ATBD-8: To compute grid ECV products

10.1. Selected altimeter standards

An objective analysis method has been selected.

Name	Description	Mission applicability
Monthly mapping algorithm	Mapping procedure using optimal interpolation with realistic correlation functions is applied to produce SLA maps at a given month	All missions

10.2. Function

To compute the MSLA grid from multi-mission along track Sea Level Anomalies

10.3. Algorithm Definition

10.3.1. Input data

- Geophysical parameters
 - The input along track SLA measurements are filtered out in order to remove the instrumental noise and the small spatial scales that cannot be mapped due to the capabilities of the observation system (altimeter). Then a subsampling of the data is made in agreement with the filtering processing (Ducet et al., 2000).
- Processing parameters
 - Objective analysis parameters
- Correlation parameters
 - Long Wave Length spatial and temporal correlations for all available missions
 - Instrumental noise for all available missions
 - Oceanic spatial and temporal correlations

10.3.2. Output data

- Multi mission MSLA grid at $1/4^\circ$ resolution on a $1/4^\circ$ on Cartesian grid

10.3.3. Mathematical statement

A mapping procedure using optimal interpolation with realistic correlation functions is applied to produce maps of Sea Level Anomalies (SLA) and Absolute Dynamic Topography (ADT) (respectively MSLA and MADT products) at a given date. The procedure generates one map for each altimeter mission but also a combined map merging measurements from all available altimeter missions (Ducet et al., 2000). Combining data from different missions significantly improves the estimation of mesoscale signals (Le Traon and Dibarboure, 1999), (Le Traon et al., 2001), (Pascual et al., 2006).



The basic algorithm used for the mapping procedure is described in Le Traon et al. 1998. The main assumptions and equations are recalled hereafter.

The aim is to estimate SLA values on a regular grid and at a fixed time tag, given along track SLA observations unequally distributed. Bretherton et al. 1976 have shown that the best least square linear estimate is given by:

$$\theta_{est}(x) \sum_{i=1}^n \sum_{j=1}^n A_{ij}^{-1} C_{xj} \phi_{obsi} \quad \text{Eq 10.1}$$

where:

- $\phi_{obsi} = \phi_i + \varepsilon_i$ are the n observations ϕ_{obsi} of the true field ϕ_i
- A_{ij} is the covariance term between observations i and j
- C_{xj} is the covariance term between the true field at point x and the observation j

This equation is also expressed under a matrix form:

$$X_{est} = CA^{-1}X_{obs} \quad \text{Eq 10.2}$$

The matrixes A and C are filled with empirical and theoretical knowledge of the oceanic signal correlations and the error characteristics.

The covariance matrix A which contains the correlation between the observations can be modelled by the following terms:

$$A_{ij} = \langle \phi_{obsi} \phi_{obsj} \rangle = \langle \phi_i \phi_j \rangle + \langle \varepsilon_i \varepsilon_j \rangle \quad \text{Eq 10.3}$$

The covariance vector between the oceanic signal and the observations is given by the following equation, assuming the measurement errors are uncorrelated with oceanic signal:

$$C_{xj} = \langle \theta(x) \phi_{obsj} \rangle = \langle \theta(x) \phi_j \rangle \quad \text{Eq 10.4}$$

Once the correlation of the oceanic signal is well characterised, one has to add the measurement error characteristics. In this case, the error is considered as :

- instrumental noise which is represented by a white noise of a chosen magnitude. This term only adds a constant term to the diagonal of matrix A .
- LWE term which represents the correlated long wavelength errors that exist on the same track of the same cycle of observations. Spatial variations are taken into account for this term.

Several improvements were made compared to the version used by (Le Traon et al., 1998). An improved statistical description of sea level variability and noise is used. Covariance functions including propagation velocities that depend on geographical position were thus used. For each grid point, the zonal and meridional spatial scales, the time scale and the zonal and meridional



propagation velocities were adjusted from five years of TP+ERS combined maps. In addition to instrumental noise, a noise of 10% of the signal variance was used to take into account the small scale variability which cannot be mapped and should be filtered in the objective analysis.

Long wavelengths errors (LWE) due to residual orbit errors but also tidal or inverse barometer errors and high frequency ocean signals were also derived from an analysis of TP and ERS data.

This method also allows estimating the error variance associated to the estimated field. The error variance is given by:

$$e^2(x) = C_{xx} - \sum_{i=1}^n \sum_{j=1}^n C_{xi} C_{xj} A_{ij}^{-1} \quad \text{Eq 10.5}$$

In the case of SLA mapping, the objective analysis is called ‘sub optimal’ because of the very high amount of measurements, which leads to select only the data the closest to the point where the SLA is estimated. The data selection is done depending on the correlation lengths of the oceanic signal and of the measurement noise. The best trade-off has to be found between the optimal data selection and the size of the correlation matrix A (the size is the number of observations) to be inverted.

10.4. References

Bretherton, F. P., Davis, R. E., and Fandry, C. B., (1976): A technique for objective analysis and design of oceanographic experiment applied to MODE-73. *Deep-Sea Research*, 23:559-582

Ducet, N., P.-Y. Le Traon, and G. Reverdin, 2000: Global high resolution mapping of ocean circulation from TOPEX/Poseidon and ERS-1 and -2. *J. Geophys. Res.*, **105**, 19477-19498.

Le Traon, P.-Y., & Dibarboure, G. (1999). Mesoscale mapping capabilities of multiple-satellite altimeter missions. *Journal of Atmospheric and Oceanic Technology*, 16(9), 1208-1223.

Le Traon, P.-Y., G. Dibarboure and N. Ducet (2001). Use of High-Resolution Model to Analyze the Mapping Capabilities of Multiple-Altitude Missions. *JAOT*, 18, pp. 1277-1288.

Pascual, A., Y. Faugère, G. Larnicol, P.-Y. Le Traon (2006). "Improved description of the ocean mesoscale variability by combining four satellites altimeters." *Geophys Reseach Letters* 33(doi:10.1029/2005GL024633).



11. ATBD-9: To compute the mean sea surface height

11.1. Selected altimeter standards

The DTU15 MSS has been selected in order to favour the Arctic Ocean which is an area of main interest for climate studies. On the other hand, the use of the DTU15 MSS instead of CNES/CLS 2011 MSS reduces the SLA performances in the open ocean which could have an impact on mesoscale applications (Algorithm Selection Meeting Executive Summary, 2015).

Name	Description	Mission applicability
DTU15 Mean Sea Surface	The mean sea surface is the displacement of the sea surface relative to a mathematical model of the earth and it closely follows the geoid. Amplitudes range between +/- 100 meters. DTU15 Ocean wide Mean Sea Surface height (relative to the Ellipsoid) has been mapped with a resolution of 1 minute by 1 minute corresponding to 2 minute by 2 minute resolution at Equator (ftp.spacecenter.dk/pub/MSS)	All missions

11.2. Function

To compute the height of the mean sea surface (MSS) and the associated accuracy at the location of the altimeter measurement, from the MSS input file.

11.3. Algorithm Definition

11.3.1. Input data

- Location:
 - Latitude of the measurement
 - Longitude of the measurement
- MSS value and accuracy (geographical grid, SAD)
- Processing parameters (SAD):
 - Interpolation window size
 - MSS offset

11.3.2. Output data

- Height of the mean sea surface above the reference ellipsoid.
- MSS interpolation flag
- MSS accuracy



11.3.3. Mathematical statement

The height of the MSS is computed at the altimeter measurement (Andersen et al., 2015) using a squared window of $N \times N$ MSS grid points (typically $N = 6$) centred on the altimeter point. Spline functions are calculated within the window as function of grid point latitude for each MSS column. Each of these spline functions is evaluated at the altimeter latitude. The resulting values are then used for calculating a spline function of grid point longitude. The height of the MSS is derived by evaluating the spline at the altimeter longitude. When one MSS grid point has a default value (grid point over land), then a lower N value is tried. If spline interpolation fails (because $N < 4$), then bilinear interpolation is performed. An offset may be added to the computed height of the MSS.

A MSS flag is also derived. It addresses the quality of the interpolation by providing the number of grid cells used during the spline (or bilinear) interpolation process. The accuracy is also provided at the location of the measurement by the MSS accuracy map (calibrated formal errors) using a bilinear interpolation.

11.4. References

- Algorithm Selection Meeting Executive Summary - SL_cci Phase II (26-27 November 2015). CLS-SLCCI-15-0015, SLCCI-MM-042. http://www.esa-sealevel-cci.org/webfm_send/400
- Andersen, O. B. and P. Knudsen (2009), DNSCO8 mean sea surface and mean dynamic topography models, *J. Geophys. Res.*, 114, C11001, doi:10.1029/2008JC005179.
- Andersen, O. B., G. Piccioni and P. Knudsen 2015. The DTU15 MSS (Mean Sea Surface) and Associated MDT (Mean Dynamic Topography) Focusing on Arctic Issues and Development. OSTST, 2015. [http://meetings.avisio.altimetry.fr/programs/abstracts-details.html?tx_ausyclsseminar_pi2\[objAbstract\]=1694&cHash=c191e0e1e8fd747b06d2213ab1bd925d](http://meetings.avisio.altimetry.fr/programs/abstracts-details.html?tx_ausyclsseminar_pi2[objAbstract]=1694&cHash=c191e0e1e8fd747b06d2213ab1bd925d)
- Hernandez, F. and P. Schaeffer, 2000: Altimetric Mean Sea Surfaces and Gravity Anomaly maps inter-comparisons AVI-NT-011-5242-CLS, 48 pp. CLS Ramonville St Agne.